Sea Ice variability and Atmospheric forcing in the Arctic North Atlantic.

Eduardo Blanchard Wrigglesworth
Girton College
Supervisor: Professor Julian Dowdeswell
June 10th, 2005

This Dissertation is for the Degree of Master in Philosophy in Polar Studies

Declaration

I declare that this is my own unaided work, and that the length of this report does not exceed 20,000 words

Eduardo Blanchard Wrigglesworth

Acknowledgements

I am especially grateful to Dr Fabian Mager, for instructing me in the fine art of computer programming. His patience and understanding were boundless. Thanks are also due to Dr Jian Yang for assistance with the use of GrADS, and Professor Graf for enlightening discussions. I would also like to thank Dr Cavalieri and Dr Widell who provided some of the necessary data.

Contents

Introduction

Sea ice is an important climate parameter that serves to modulate the Earth´s albedo, the heat exchange between the Ocean and the Atmosphere, and the oceanic circulation through the forcing of the thermohaline circulation. Sea ice in the Arctic and adjacent seas has received increasing attention in recent decades as a result of anthropogenic climate change which predicts the highest 21st century temperature rise to occur over the Arctic. Thus present day changes in sea ice cover may be a sign of global warming. One of the important elements is the Fram Strait ice flux, the main export path for sea ice out of the Arctic. Variations in this sea ice export have been studied in the context of atmospheric variability. In this work, I make use of observational data that has recently become available (Widell et al, 2003) to study in greater depth such a connection.

Sea ice fluctuations are mainly driven by atmospheric (e.g. temperature, wind) and oceanic (e.g. salinity, sea surface temperatures) factors. Global atmospheric circulation can be described by negative and positive anomalies of atmospheric pressure which extend across several hundreds to thousands of kilometres and correlate with surface weather phenomena (e.g. van Loon and Rogers, 1978; Wallace and Gutzler, 1981). Thus, temporal and spatial variations in weather variables, such as temperature and precipitation, may be related to variations in atmospheric circulation (i.e. mesoscale climate). This makes it possible to study the relation between sea ice fluctuations and variations in atmospheric circulation. Winter atmospheric circulation and climate over the North Atlantic is dominated by the North Atlantic Oscillation (Hurrell, 1995), the 'tendency for pressure to be low near Iceland when it is high near the Azores and south-west Europe' (Walker and Bliss, 1932). At the same time, several studies (e.g. Baldwin and Dunkerton, 2001) have shown that the polarity of the winter NAO index and the patterns of tropospheric teleconnectivity depend on the state of the stratospheric polar vortex. The North Atlantic is also the area of highest interannual sea ice variability in the northern hemisphere. In this work, the link between the NAO index and

sea ice fluctuations is studied, together with the influence that the stratospheric polar vortex has on such fluctuations.

Data

Sea Ice

Sea ice data (Armstrong and Brodzik, 2002) was obtained from the National Snow and Ice Data Center in Boulder (University of Colorado), Colorado , US in the form of the Northern Hemisphere EASE-Grid Weekly Snow Cover and Sea Ice Extent Version 2 data set. Sea ice extent in this dataset is available at weekly intervals for October 1978 through June 2001. Data is available continuously apart from three periods, one week in August 1984, two weeks in April 1986, and 5 weeks between December 1987 and January 1988. The data originates from satellite passive microwave observations from the special sensor microwave/imager (SSM/I) on board the Defence Meteorological Satellite Program (DMSP) series of satellites as well as the scanning multichannel microwave radiometer (SMMR) on the Nimbus-7 satellite. The Nimbus-7 satellite was launched by NASA in October 1978, and the SMMR operated successfully until summer 1987 when it was succeeded by satellites of the DMSP. The SSM/I observations are taken on a daily basis, whereas the SMMR observations are bi-daily. The use of microwaves to observe ice conditions allows continuous monitoring, even during the polar night and during periods with persistent cloud cover where traditional visible and infrared techniques have limited use. The instruments measure the amount of thermal microwave radiation emitted by the surface of the Earth, also known as the brightness temperature. The spectral composition of this emission differs substantially from ice-free to ice-covered ocean, and from multi-spectral measurements it is possible to derive the ice concentration in each cell. Cells in which the ice concentration exceeds 15% are considered to be ice covered. Although other figures have sporadically been used (e.g. 10 or 20%),

validation studies such as the NASA DMSP SSMI Sea Ice Validation Program have shown that the ice edge location, defined as the position of the initial ice bands, correspond to an SSMI ice concentration of 15% (Cavalieri et al 1991). Because of the satellite orbits and the instrument swath widths, the SMMR data do not extend poleward of 84.6 latitude and the SSMI data do not extend poleward of 87.6 latitude. While it is usually assumed that there is full ice coverage, 100%, north of 84.6 N (e.g. Gloersen and Campbell, 1991), it does not affect the present study as all areas are southward of 84.6 N.

Atmospheric data

I used reanalysis data of geopotential height from the National Centres for Environmental Prediction / National Centre for Atmospheric research. The data is available for the whole globe on a 2,5° by 2,5° grid from 1958 to 2004. Gridded Analysis Data Software, or GrADS, developed by the Centre for Ocean-Land-Atmosphere Studies (COLA), is used in the production of the pressure maps. The Generic Mapping Tools software, or GMT, developed by Paul Wessel (University of Hawaii, USA) and Walter Smith (Laboratory for Satellite Altimetry, NOAA, USA), is used in the production of sea ice maps and boxed areas.

Fram Strait

Introduction

Fram strait lies between the Svalbard Archipielago and northeastern Greenland, at around 80N and 16W to 10 E. It is the main gate for export of Arctic sea ice, and the magnitude of the ice export is considered to provide an estimate of net ice production in the Arctic Ocean (e.g. Vinje et al, 1998). The bulk of this exported ice originates north of the East Siberian

and Laptev Seas for all months except for the summer months when the provenance is north of Greenland. This marked change in provenance results from the varying mean monthly geostrophic wind, backing from northeast in January to northwest in June. Figure 1 shows mean sea level pressure (SLP in the following) for all seasons (winter: December to February; spring: March to May; summer: June to August, and autumn: September to November) from 1958 to 2003.

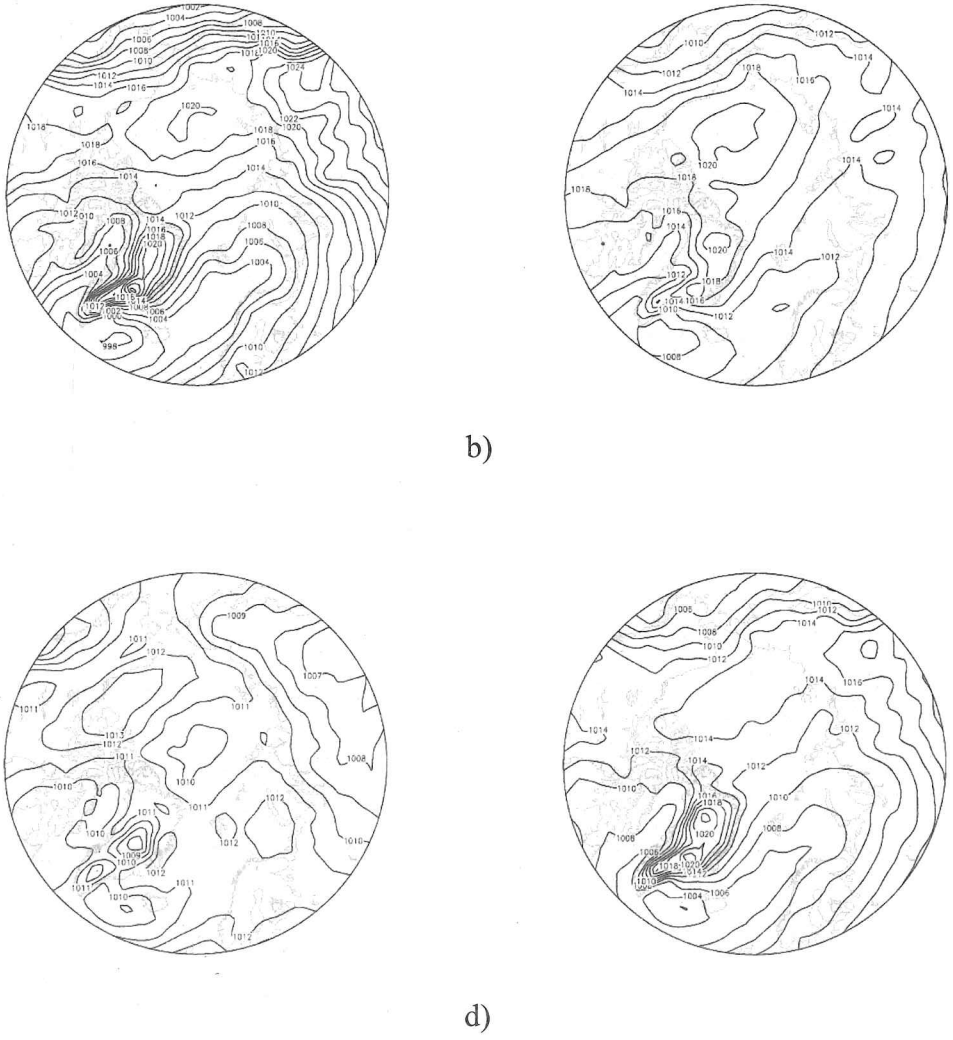

a) b)

c) d)

Figure 1. Seasonal mean SLP for the Arctic and adjacent regions: a) winter, b) spring, c) summer, d) autumn.

The seasonal mean SLP shows how for most of the year, mean circulation in the Artic ocean is driven by two conspicuous features, the Barents-Norwegian sea trough of low pressure which developes off the Icelandic low, and the Beaufort Sea high, an area of high pressure to

the north of Alaska that is developes off the Siberian high during winter months. Thus, the mean geostrophic wind flow over the Arctic ocean is from Siberia towards the Canadian high Arctic / northern Greenland with a gyre that forms over the Beaufort sea. Over Greenland, an area of high pressure is present for all non-summer months, which in combination with the low pressure area over the Norwegian/Barents region, acts to drive the East Greenland current (EGC in the following). The major exception to this general pattern are the summer months, when the Greenland high and Barents Low are replaced by opposite features (ie a Greenland low and Barents high) and an area of low pressure forms over the pole. With such a configuration, the northeasterly winds in the Fram Strait are replaced by westerly/northwesterly winds. Note how the summer circulation is weak and the contours in Fig. 1c are 1mb to aide visualisation. Meanwhile, the average time it takes time from different locations in the Arctic Ocean to reach the Fram Strait varies from 6 years for ice from the southern Beaufort Sea to 1 year for ice north of Svalbard (Vinje et al, 1998). Ice passing through the Fram Strait is then carried southward along the eastern coast of Greenland in the EGC with minor contributions from glaciers and locally formed sea ice. As it travels south it melts thereby acting as an input of fresh water to the Greenland sea. The Greenland sea is only one of four areas in the world ocean where ventilation occurs through open convective renewal of intermediate and deep waters in winter, the others being the Labrador Sea, the western Mediterranean and the Ross and Weddell seas in the southern hemisphere (Wadhams, 1999), and it is this input of fresh water that modulates the North Atlantic thermohaline circulation (Mauritzen and Häkkinen, 1997). By its variability, the Fram Strait ice flux in considered both to influence global climate and provide a climate signal itself, and it has received increasing interest in the light of the reported climate changes in the Arctic.

Ice export across the Fram Strait is primarily driven by the wind field in the area, northerly winds enhancing ice flux while southerly winds reduce the flux and even reverse it. Air pressure gradient across the Fram Strait determines the wind field.

The annual variation in the air pressure distribution in the Arctic Ocean and the Nordic Seas thus determine the ice flux through the Fram Strait (e.g. Vinje, 2001). Figure 2 shows the mean winter (December to February) SLP associated with the greatest and lowest winter FS ice export years and difference between composites.

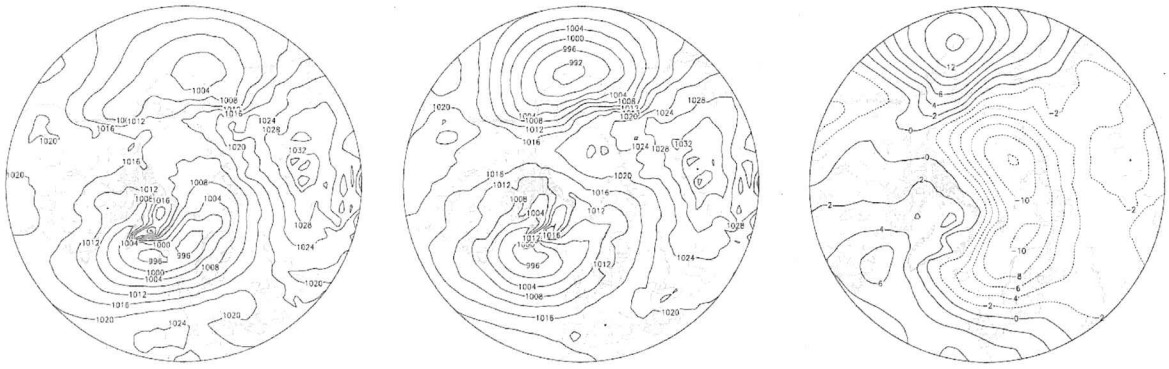

i) ii) iii)

Figure 2. Mean winter SLP for i) high FS ice export years, ii) low FS ice export years, and iii) difference between high and low years.

These large scale variations in air pressure can be linked to climatic indexes that represent modes of variability of the atmospheric circulation. The main mode of variability for the North Atlantic and the Nordic seas region is the North Atlantic Oscillation (NAO, Walker, 1923), while that for the Arctic is the Arctic Oscillation (AO, Thompson and Wallace, 1998). While the AO is a circumhemispheric phenomenon, the NAO may be viewed as a regional imprint of the AO, and it has been postulated that they are both representations of the same physical process (eg. Ambaum et al, 2001; Rogers and McHugh, 2002). The NAO and AO are nearly indistinguishable in the time domain: the correlation coefficient of monthly anomalies over the Northern Hemisphere cold season (November to April) is 0.95 (Deser, 2000). These patterns describe a large proportion of tropospheric variability especially during the winter half of the year, and over the last decade or so there has been a considerable

amount of research into the link of these modes of climatic variability and Fram Strait ice flux.

Fram Strait ice measurements

Studies of Fram Strait ice flux and atmospheric variability are hindered by the lack of comprehensive ice thickness observations prior to the 1990s. While ice area flux may be calculated from satellite observations by tracking ice floes in sequential images (e.g. Kwok and Rothrock, 1999) and buoy drifts (Vinje et al, 1998), and the width of the ice stream can be measured from ice maps, ice volume flux requires in situ sea ice thickness measurements across the strait (Vinje et al, 1998). Satellite observations of sea ice and thus sea ice area flux are available since 1978, whereas continuous sea ice thickness data in the fram strait is available since 1990 (Vinje et al, 1998). Earlier sea ice thickness measurements are available from submarine cruises but are sporadic and generally from different locations within the Fram Strait (e.g .Wadhams 1990). Reconstructions of Fram Strait ice export have been made from historical observations of multiyear ice in southwest Greenland for the period 1820-2000 (Schmith and Hansen, 2003), while dynamic-thermodynamic models have been used to simulate FS ice export (e.g. Häkkinen and Geiger, 2000; Hilmer, 2001). In this work, model Fram Strait ice export data is used extensively, as these provide a time series long enough for meaningful statistical analysis. The Häkkinen and Geiger model (Häkkinen in the following) is a coupled ice-ocean model forced by monthly surface wind and air temperature data derived from the NCEP/NCAR reanalysis project. The Hilmer model is forced by daily surface wind and temperature data also derived from the above NCEP/NCAR source.

Observational ice export measurements

The first successful, year-long ice thickness series was obtained in the East Greenland ice drift stream in 1987-1988 at 75N, while the first deployment in Fram Strait was made in 1988 (Vinje et al, 1998). It is only since 1990 that annual time series have been obtained

regularly from this latitude. The only direct measurements of sea ice velocities have been measured since 1996 using moored Doppler current meters (Widell et al, 2003). Parametrization of the ice flux through the strait by the difference in SLP has been used by a number of authors (e.g. Vinje et al, 1998). The most complete set of observational data comes from Widell et al (2003). A comparison between the Widell data and the Häkkinen and Hilmer model results is shown in Fig. 3.

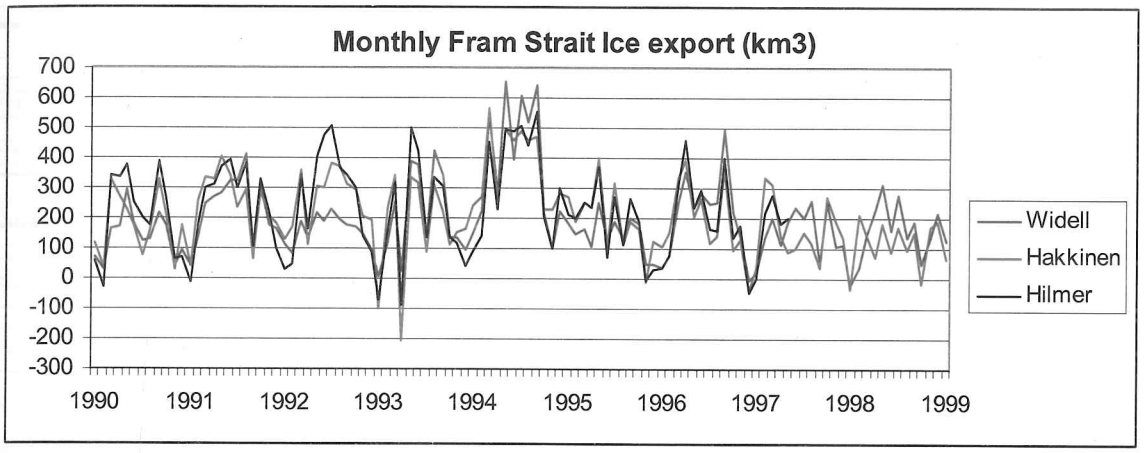

Figure 3. Observational (Widell) and model (Häkkinen and Hilmer) data for FS ice export, August 1990 to August 1999.

The Häkkinen model describes 59% of the variance while the Hilmer model explains 68%. Both models accurately capture the seasonal variation of FS ice flux and the large enhanced flux of winter 1994/95, but large differences arise, most notably during the winter of 1992/1993. The models do not capture variations in sea ice thickness or ocean circulation, which lead to the differences between the model and observational data. Table 1 shows the correlation between the Widell, Häkkinen and Hilmer timeseries.

Table 1		
Correlation between observed and modelled Fram Strait ice export. All values are significant at the 0.5% level		
Compared variables	1990-1997	1990-1999
Widell-Häkkinen	0,78	0,77
Widell-Hilmer	0,83	
Hilmer-Häkkinen	0,88	

Table 2 shows the monthly averages and standard deviations for observed and modelled data.

Table 2			
Monthly average Fram Strait ice export (km3) with standard deviations (parenthesis)			
	Widell (1990-99)	Häkkinen (1951-00)	Hilmer (1958-97)
January	252 (97)	230 (127)	274 (140)
February	259 (145)	236 (140)	275 (125)
March	273 (144)	245 (122)	297 (144)
April	264 (195)	223 (107)	273 (114)
May	190 (75)	170 (92)	210 (88)
June	114 (46)	141 (118)	158 (107)
July	116 (76)	123 (102)	89 (99)
August	71 (67)	98 (102)	59 (90)
September	119(61)	201 (95)	153 (88)
October	249 (123)	256 (107)	260 (94)
November	189 (105)	237 (117)	295 (122)
December	316 (140)	265 (124)	317 (119)
Annual	2445 (706)	2359 (654)	2660 (524)

Fram Strait ice flux peaks in the winter months, with a maximum in December and a secondary maximum in March, which shows both in observational and model data. The lowest values are recorded in summer, with a minimum in August. While the models and observed data show an annual export of around 2500km3, there is some disagreement in the seasonality of the flux, the Häkkinen model showing a less pronounced seasonality. The standard deviations show higher variability during winter than summer, which is to be expected given the stronger atmospheric circulation in winter. While the Widell data is too short to make assessments on variations in standard deviation, it does seem that the models in general overestimate the amount of summer flux variability.

Fram Strait Ice Flux and the NAO index

A variety of results have been obtained by different authors studying the link between the NAO index and Fram Strait ice flux (see Table 3).

Table 3

Correlation between NAO index and Fram Strait Ice export

Author	Time period	Season	Correlation
Kwok & Rothrock (1999)	1991-1996	December-March	0.56
Dickson et al (2000)	1976-1995	December-March	0.80
Hilmer and Jung (2000)	1958-1977	December-March	0.1
	1978-1997		0.7
Vinje (2001)	1962-1978	December-March	-0.3
	1950-2000		0.1
Cavalieri (2002)	1958-1979	January	0.1
	1980-1997		0.17

While generally positive, significant correlations are found for the period spanning the late 1970s to late 1990s, the correlation loses significance and approaches zero when the time series are extended to the 1950s (e.g. Hilmer and Jung, 2000). Figure 4 shows the winter SLP field over the Northern Hemisphere when the NAO is in its positive mode (greater than + 1 standard deviation) and negative mode (lower than -1 s. d.) and the difference between the two composites; figure 5 shows a time series for the winter (December to March) NAO series, updated from Hurrell (1995).

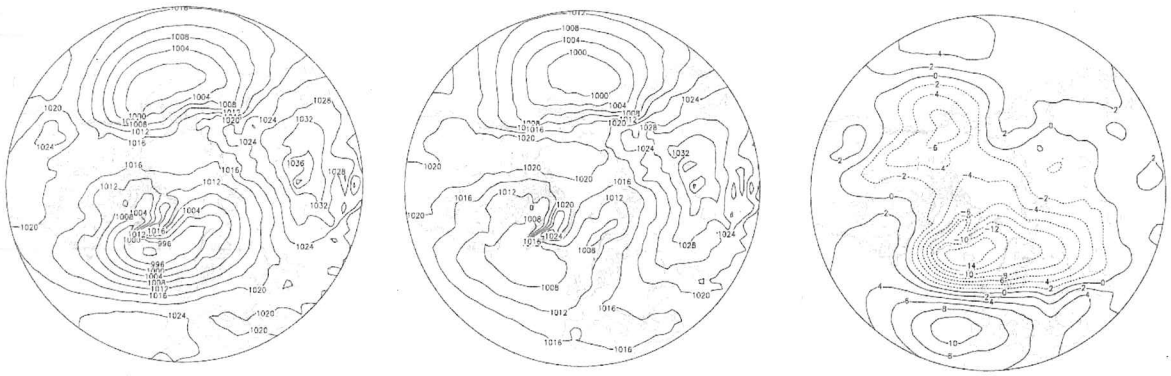

i) ii) iii)

Figure 4. Mean winter SLP for i) positive NAO, ii) negative NAO, iii) difference between composites.

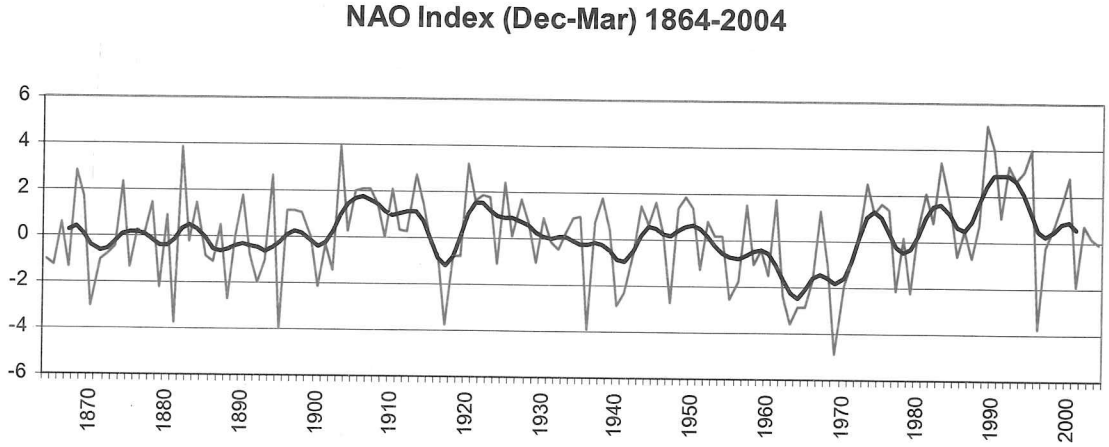

Figure 5. Mean winter NAO Index for 1864-2004 with a low pass (7 weight) filter

Several authors have postulated that the NAO mainly exerts its influence on the Fram Strait region when in a positive phase, as the Icelandic Low extends into the Barents Sea, the strength of this low pressure trough increasing with a higher positive NAO index. Conversely, when the NAO is in its negative phase, the air pressure field over the Fram Strait is less constrained to the NAO index. As the NAO has been mainly in a positive phase over the recent decades, this would explain the significant positive correlation found for the latter period of the 20th century. Dickson et al (2000) show that during extreme negative NAO index years such as the 1960s, an enhanced ice flux may be set up due to an anomalously strong high pressure cell over Greenland, showing a lack of correlation overall between the NAO index and Fram Strait ice export.

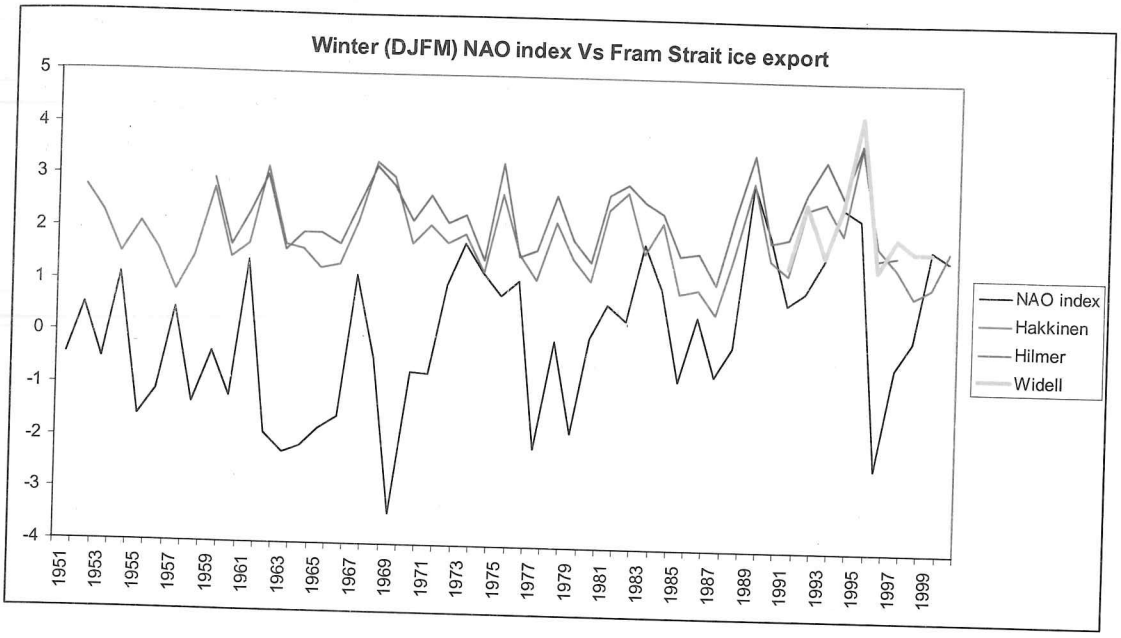

Figure 6 Winter (December to March) NAO index and Fram Strait ice export. The Fram Strait ice export values are cumulative DJFM values divided by 500 to aide visualisation.

It is clear that since the late 1970s, there has been a marked positive correlation, while prior to that there is no significant correlation (see Figure 7).

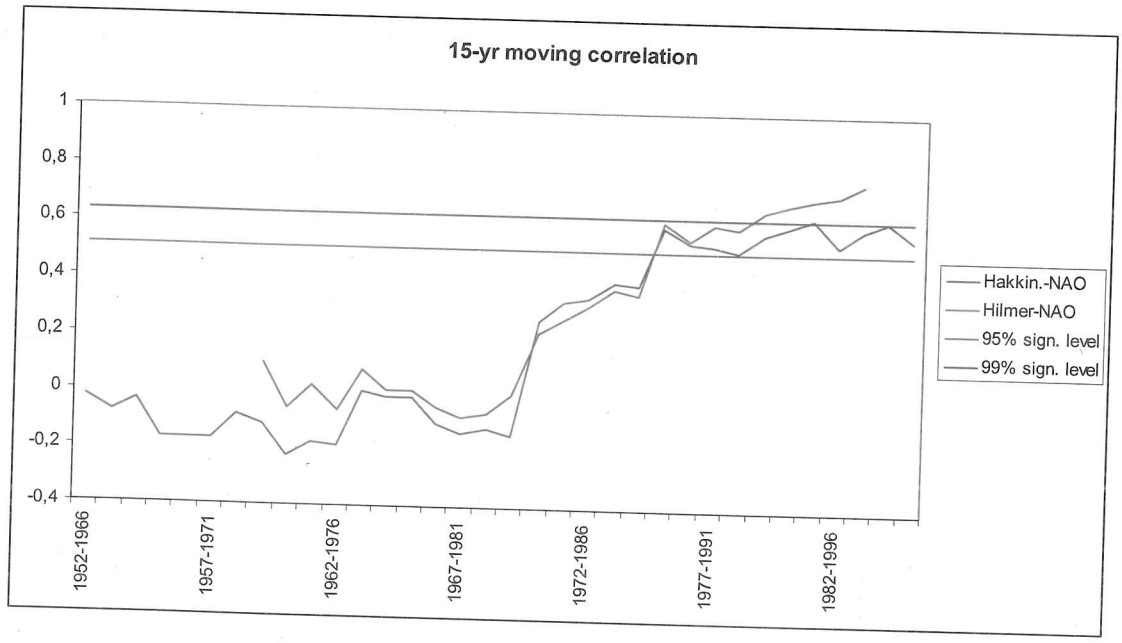

Figure 7. 15 year moving correlations for winter NAO index and FS ice export

Fram Strait Ice flux and Planetary waves

More recently, Cavalieri (2003) reported a link between FS ice export and atmospheric planetary wave phases. Planetary waves, also known as Rossby waves, depict the meandering of air masses at a planetary scale, and are numbered according to the number of peaks and troughs that they contain longitudinally. Thus, a planetary wave number 1 has one peak and one trough with a separation 180 degrees and of the same amplitude, whereas a wave number 4 will have four peaks, four troughs of the same amplitude separated 45 degrees from each other. The larger planetary waves (i.e. waves n1 and to a lesser extent wave n2) reflect changes in the strength and position of the large semi-permanent pressure systems found in the general atmospheric circulation, such as the Siberian High and Icelandic Low, the shorter planetary waves reflect the degree of blocking of the zonal circulation present. The longer waves (1, 2, and to some extent 3) are stationery, and their locations are determined by the geographical distribution of continents / oceans (wave 1) and major mountain ranges (wave 2); the shorter waves (4 onwards) tend to be transient. Whereas the phase of a wave describes the longitudinal position along which the peaks (and thus troughs) are located, the amplitude of the wave describes the amount that particular wave contributes to the general circulation. Figure 8 shows the mean wave 1 for January 1985 for all latitudes north of 45N (8.i) and for 75N (8.ii), computed by a zonal Fourier analysis of monthly averaged SLP.

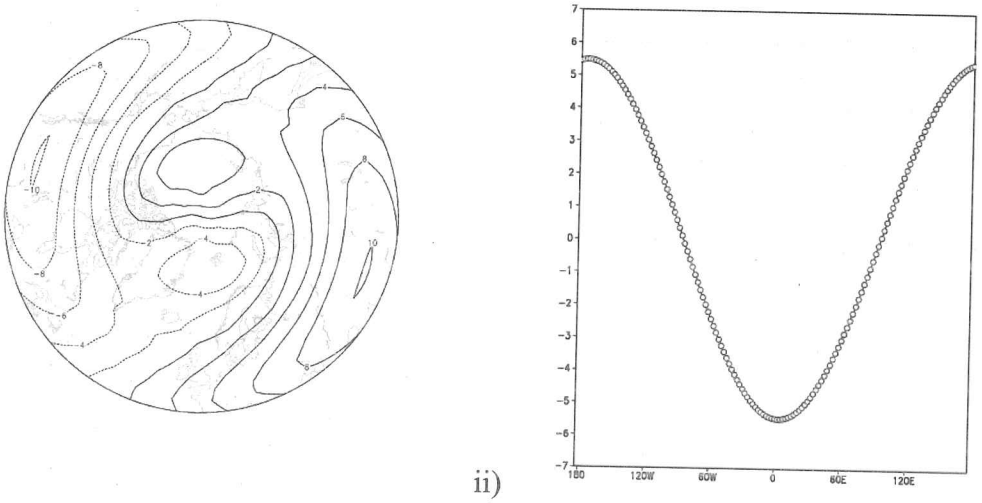

i) ii)

Figure 8. Wave 1 for Northern Hemisphere, i) north of 45N, ii) 75N.

Figure 8 shows how Wave 1 captures the location of the Siberian high, the Icelandic-Norwegian sea-Barents low pressure area and the Beaufort high.

Within an Arctic context Cavalieri and Häkkinen (2001) postulate that the atmospheric circulation patterns that emerge when waves 1 and 2 are in their extreme eastern and western positions may account for significant forcing of Arctic sea ice. Cavalieri (2002) developed this concept further and reported on a statistically significant link between the phase of wave 1 and FS ice export.

He computed the correlation for January wave 1 phase and FS ice flux to be r=0.71 for the Häkkinen model and r=0.59 with the Hilmer model, thereby wave 1 phase explaining 50% and 35% of the variance of FS ice flux respectively. The correlation figures increase to r=0.84 and r=0.77 for the Häkkinen and Hilmer models respectively when the years 1966 and 1967 are excluded, on the grounds that wave 1 was in an anomalous position. However, I performed the same analysis as Dr. Cavalieri using *his* data both in terms of wave 1 and the ice model results, obtaining a correlation of r=0.61 and r=0.54 for the Häkkinen and Hilmer models respectively, significant lower than r=0.71 and r=0.59. While Dr Cavalieri refused to comment when contacted, it is noteworthy that in his paper, he states that 'the variance explained by the wave-1 phase... is 37% and increases to 71% when the two anomalous years, 1966 and 1967, are removed'. A variance explained of 37% corresponds to r^2=0.37 which yields a value for r of 0.61, the value I obtained using Dr Cavalieri's data.

To investigate the relationship between wave 1 phase and FS ice flux further I computed the wave 1 phase for all months from 1958 to the present. This was done by performing a zonal Fourier analysis of monthly-averaged SLP over the ten degree latitude band 70-80N. My results were found to agree with Cavalieri's, validating the analysis. Table 4 shows the correlation between wave 1 phase and the FS ice export for both model results for all months of the year.

Table 4

Correlations Wave 1 phase – FS ice export. One asterisk indicates statistical significance at the 5% level, two indicate significance at the 1% level.

	Häkkinen	Hilmer
January	0,67**	0,58**
February	0,48**	0,45**
March	0,51**	0,48**
April	0,61**	0,52**
May	0,50**	0,43**
June	0,51**	0,46**
July	0,56**	0,64**
August	0,67**	0,68**
September	0,32*	0,47**
October	0,60**	0,56**
November	0,52**	0,36*
December	0,52**	0,39*

January clearly stands out as the month with the highest correlation values for the Häkkinen model, whereas for the Hilmer model, while being lower than summer months July and August, it is the highest winter month correlation. All correlations are significant to the 5% level, and most to the 1% level. These highly significant correlations are also present when computed for several combinations of winter months (see table 5), meaning that the relationship between wave 1 phase and FS ice export remains quasi-stationery throughout the winter.

Table 5

Model FS ice export correlations with Wave 1 phase, JF= January to February, JFM= January to March, DJFM= December to March, DJ= December to January, NDJFMA= November to April. All values are significant to the 1% level.

	Häkkinen	Hilmer
JF	0,56	0,51
JFM	0,55	0,50
DJFM	0,55	0,48
DJ	0,60	0,50
NDJFMA	0,53	0,44

This can also be deduced from the similarity of the lines of best fit in Figure 10 showing scatter plots for all months for both model data.

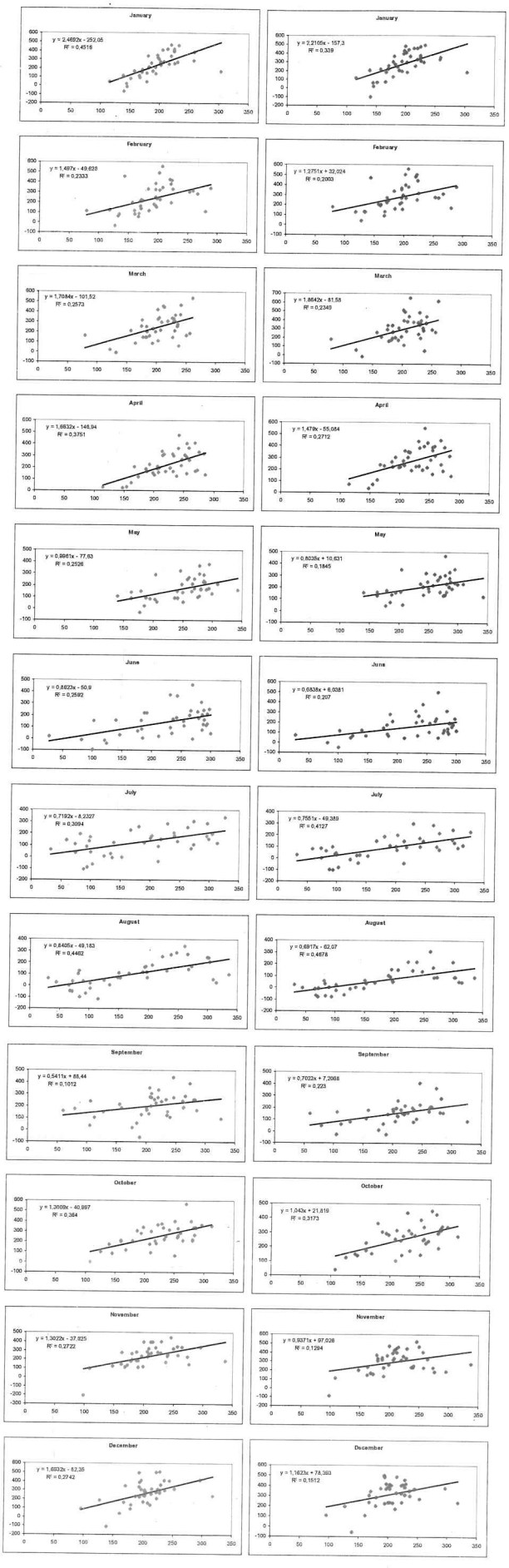

Figure 10. Monthly Scatter plots for FS ice export data and wave 1 phase, left) Häkkinen, right)Hilmer.

The increase in Fram Strait ice export with eastward displacement of Wave 1 phase can be visualised by looking at months with wave 1 phase in westerly and easterly positions. (see figure 11).

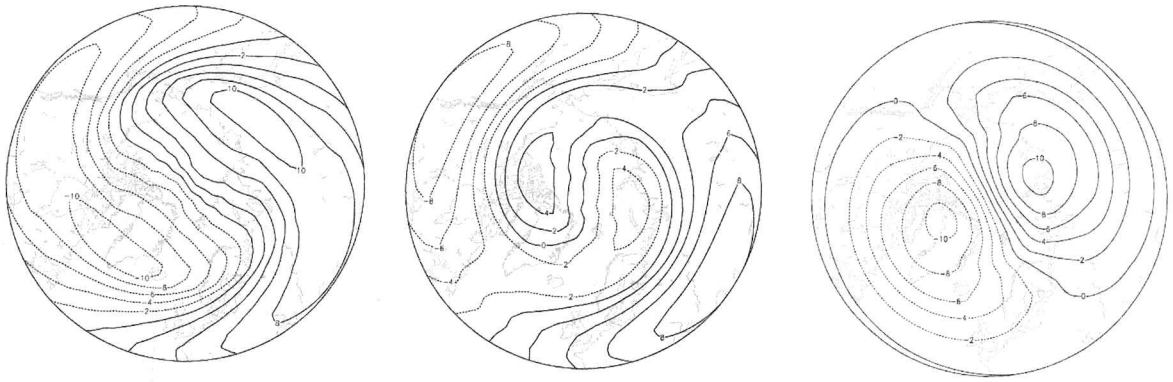

i) ii) iii)

Figure 11 Wave 1 for winters (December to February) with phase in i) westerly position (-1 standard deviation), ii) easterly position (+1 s.d) and iii) difference between the composites.

In the westerly position, the configuration of the wave 1 ridge (ie the maximum) and trough over northeastern Siberia and southern Greenland respectively result in a near zero pressure gradient over the Fram Strait. As wave 1 phase 'travels' eastward to eventually reach the configuration in Figure 11.ii, the resulting pressure gradient over the Fram Strait and thus ice export slowly increases. The difference between easterly and westerly wave 1 phase months show enhanced north-northwesterly (south-southeasterly) flow over the Fram Strait in the eastern (western) cases. It is noteworthy that the easterly position of wave 1 has an amplitude around half that for the westerly position of wave 1, indicating an enhanced (reduced) zonal circulation when wave 1 is in a easterly (westerly) position.

Anomalous easterly Wave 1 phase

From visual inspection of winter month data in figure 10 it becomes clear that all months contain what Cavalieri (2003) calls 'anomalous' wave 1 phase values greater than 250 degrees. While Cavalieri and Häkkinen (2001) relate the eastward shift of wave 1 in 1966 and 1967 to the large-scale change in atmospheric circulation in the late 1960s, Table 6 shows the years for other winter months in which the wave 1 phase exceeds 250 degrees.

Table 6

Winter months with wave 1 phase greater than 250E.

December		January		February		March	
Year	Phase	Year	Phase	Year	Phase	Year	Phase
1963	252,5	1966	257	1960	266,5	1958	256
1978	318	1967	303,5	1963	252,2	1962	260,5
1981	296	1969	258,5	1978	288,5		
				1986	280,5		
				1996	259		

For all winter months there are values exceeding 250 degrees, at a frequency varying between 2 and 5 events in the 40 year period 1958-1997. The timing of these events also seems to be random in nature, and apart from January, no other winter months show anomalous eastward values in the late 1960s. We therefore, given the number and timing of these events, postulate that these are part of the inherent variability of wave 1 and is not valid to remove them from the data series when correlating these to Fram Strait ice flux. It is to be expected for the correlation values to be lowered by these anomalous years, as an anomalous eastward phase does not lead to an anomalously high FS ice export (see Figure 10 above)

Wave 1 phase and Observational data

The link between the phase of wave 1 and FS ice export for observational data is investigated. The monthly correlation between the phase of wave 1 and observed and modelled data for FS ice export is shown in Table 7.

Anomalous easterly Wave 1 phase

From visual inspection of winter month data in figure 10 it becomes clear that all months contain what Cavalieri (2003) calls 'anomalous' wave 1 phase values greater than 250 degrees. While Cavalieri and Häkkinen (2001) relate the eastward shift of wave 1 in 1966 and 1967 to the large-scale change in atmospheric circulation in the late 1960s, Table 6 shows the years for other winter months in which the wave 1 phase exceeds 250 degrees.

Table 6

Winter months with wave 1 phase greater than 250E.

December		January		February		March	
Year	Phase	Year	Phase	Year	Phase	Year	Phase
1963	252,5	1966	257	1960	266,5	1958	256
1978	318	1967	303,5	1963	252,2	1962	260,5
1981	296	1969	258,5	1978	288,5		
				1986	280,5		
				1996	259		

For all winter months there are values exceeding 250 degrees, at a frequency varying between 2 and 5 events in the 40 year period 1958-1997. The timing of these events also seems to be random in nature, and apart from January, no other winter months show anomalous eastward values in the late 1960s. We therefore, given the number and timing of these events, postulate that these are part of the inherent variability of wave 1 and is not valid to remove them from the data series when correlating these to Fram Strait ice flux. It is to be expected for the correlation values to be lowered by these anomalous years, as an anomalous eastward phase does not lead to an anomalously high FS ice export (see Figure 10 above)

Wave 1 phase and Observational data

The link between the phase of wave 1 and FS ice export for observational data is investigated. The monthly correlation between the phase of wave 1 and observed and modelled data for FS ice export is shown in Table 7.

Table 7

Correlation between wave 1 phase and FS ice export, for Aug 1990 to Aug 1999 (Dec 1997 for Hilmer data). One asterisk indicates statistical significance at the 5% level, two indicate significance at the 1% level.

	Widell	Häkkinen	Hilmer
January	0,81**	0,90**	0,81*
February	0,11	0,59	0,46
March	0,42	0,46	0,49
April	0,59	0,79**	0,78*
May	0,33	0,67*	0,47
June	0,63	0,81**	0,78*
July	0,22	0,21	0,31
August	0,78**	0,75**	0,74*
September	0,21	0,44	0,77*
October	0,32	0,62	0,27
November	0,29	0,72*	0,62
December	-0,28	0,31	-0,03

While it is necessary to regard these results with caution due to the short length of the timeseries, it is noteworthy that in general the observational data shows a lower correlation with Wave 1 phase than the model data. At the same time, the general monthly fluctuations in the degree of correlation between the two variables for observational data follow a similar pattern to the model data. Thus, both the modelled and observed FS ice export data show correlation maxima in January. Comparing with table 4 above, there is a correspondence between months with large correlation values (e.g. April, June, August). Only during January and August there is a significant correlation between observed (Widell) FS ice export data and the phase of wave 1.

Fram Strait ice export and Svalbard glacier mass balance

A significant correlation is found between Fram Strait ice flux and glacier mass balance for two glaciers in Svalbard. The mass balance of a glacier is the difference between the mass gained from sources such as snowfall and avalanches and the mass lost by processes such as sublimation and melting. For glaciers outside the tropics and thus with clearly defined winter and summer periods, the mass balance of a glacier may be divided into two parts: the winter and summer balances. The winter balance (b_w) may be defined as the winter net accumulation of the glacier and the summer balance (b_s) as the summer net mass loss of the glacier. The net balance (b_n) is defined as $b_n = b_w + b_s$. The lengths of the summer and winter periods are dependant on the geographic location of the glacier, and more specifically the mean air temperature. Glaciers in cold climates tend to have long winter seasons with a short 2-3 month ablation period starting in early to mid June and ending towards the end of August-early September. Winter mass balance is dependant on winter precipitation while summer mass balance tends to be driven by summer temperatures. To perform meaningful statistical analysis on glacier mass balance, the mass balance record must span a sufficiently long period. The choice of a cut-off period length (below which one may choose to discard a mass balance record) is arbitrary and dependant on the records available. Two glaciers are selected for study, Midtre Lovenbreen and Austre Broggerbreen (see Table 8 for geographical data).

Table 8

Geographical data for the Svalbard glaciers, including time span of mass balance measurements.

Glacier	Position (Lat, long)	Altitude (m)	Observation period
Austre Broggerbreen	78°54'N, 11°50'E	40-600	1967-1997
Midtre Lovenbreen	78°53'N, 12°04'E	50-650	1968-1997

Winter Mass Balance

In a study on glacier mass balance and atmospheric variability, Blanchard (2003) showed that high winter accumulation in Svalbard occurs when the low pressure trough in the Nordic seas and the Barents secondary low are weakened and displaced slightly westward. This

allows the advection of the warm sector of moisture bearing Atlantic cyclonic systems over Svalbard, enhancing precipitation. Low accumulation years are characterised by a weak Icelandic low and a deep secondary low to the northwest of Scandinavia, with a trough extending towards Novaya Zemlya. The position of the Secondary Low and the trough towards Novaya Zemlya inhibits the penetration of mild humid Atlantic air masses into the higher latitudes where Svalbard is located, and the mean flow is easterly, cold and dry. Figure 13 shows the SLP distribution for winters with mass balance in the upper quartile (large winter mass balance) and lower quartile (low winter mass balance) for Midtre Lovenbreen.

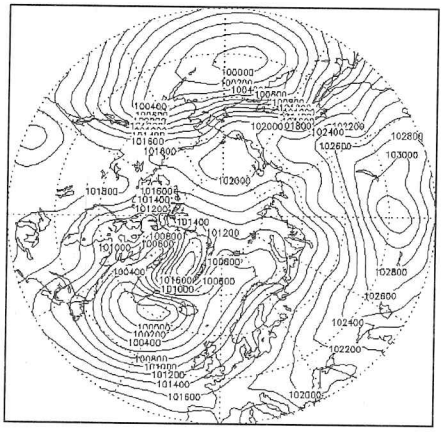

i)

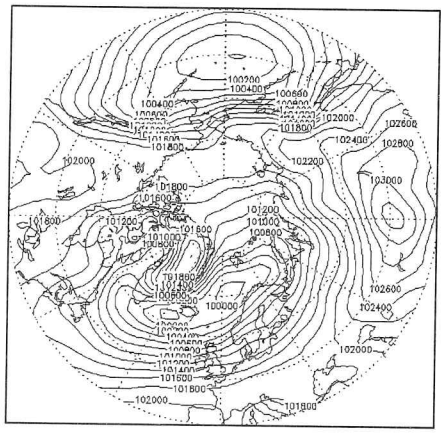

ii)

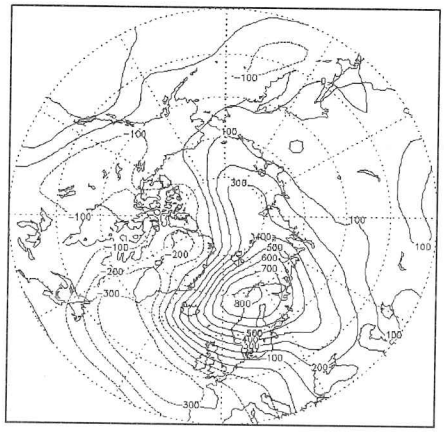

iii)

Figure 13. Mean winter (December to February) SLP for i) winters with high winter accumulation, ii) low winter accumulation, and iii) difference between the composites (extracted from Blanchard, 2003; units in hundredths of millibar)

The pressure distribution maps for Austre Broggerbreen (not shown here) are similar to those for Midtre Lovenbreen. It can be seen in 13.c. that high winter mass balance years show an enhanced southerly geostrophic flow over the Fram Strait region, whereas during low winter mass balance years an enhanced northerly air flow is set up. Considering the pressure distributions that lead the variability in the FS ice export signal (see Figure 2 above), we can theorize that high FS ice export years will be associated with low winter mass balance for Svalbard glaciers and viceversa.

Table 8

Correlation between model FS ice export and winter mass balance for Svalbard glaciers. All values are significant to the 1% level.

Hilmer FS model output

	JFM	DJF	DJFM	NDJF	NDJFM	DJFMA	NDJFMA
Mid. Lov.	-0,41	-0,42	-0,42	-0,49	-0,48	-0,41	-0,47
Aus. Brog.	-0,47	-0,52	-0,50	-0,55	-0,54	-0,48	-0,51

Häkkinen FS model output

	JFM	DJF	DJFM	NDJF	NDJFM	DJFMA	NDJFMA
Mid. Lov.	-0,51	-0,54	-0,55	-0,55	-0,58	-0,55	-0,58
Aus. Brog.	-0,54	-0,59	-0,59	-0,57	-0,60	-0,58	-0,59

Table 8 shows the correlation coefficients between the Hilmer and Häkkinen model results and winter mass balance for Midtre Lovenbreen and Austre Broggerbreen. All values are significant to the 1% level. Several different monthly averages are computed to find the time period that yields the highest correlations. These are produced by early to mid-late winter

months, November to February or March. Figure 14 shows the time series for November to March Hilmer model FS ice export and winter mass balances for both glaciers.

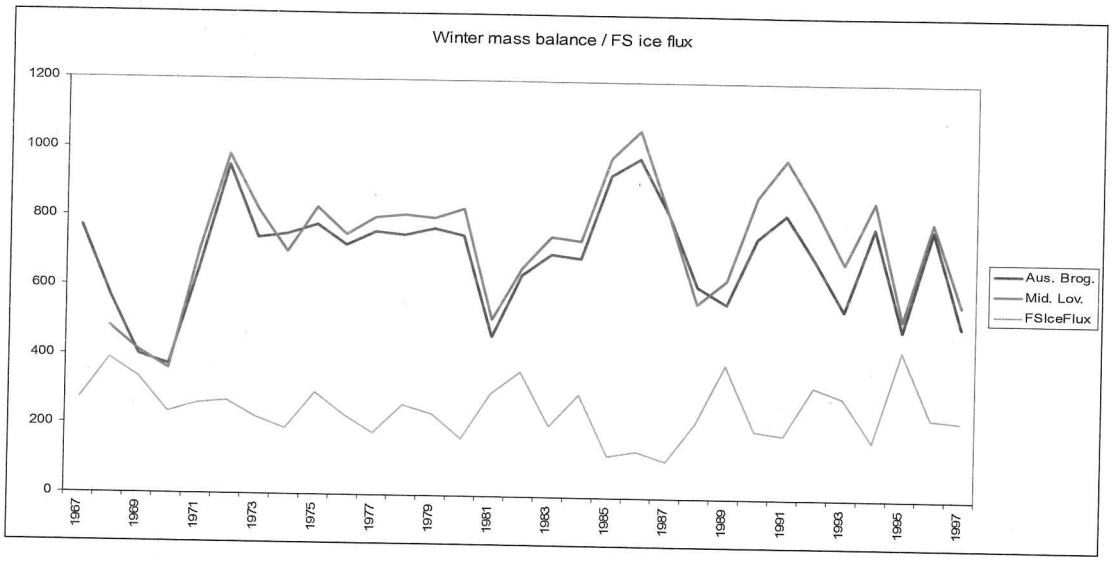

Figure 14. Model (Hilmer) FS ice export and Svalbard winter mass balance. Winter mass balance is in units of millimetres of water equivalent.

The anticorrelation of FS ice flux and winter mass balance is rather remarkable, especially since the late 1970s. Figure 15 shows 15 year moving correlations.

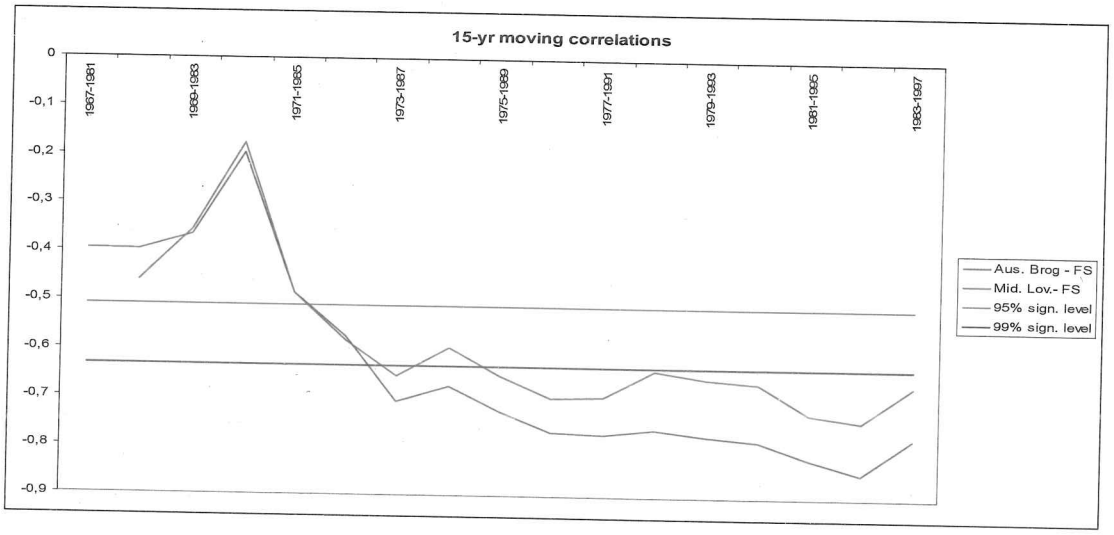

Figure 15. 15 year moving correlations for model (Hilmer) FS ice export and Svalbard winter mass balance.

Confirming above visual inspection, the correlations do not become significant until the mid to late 1970s. In the second half of the period, both correlations are significant to a 99%

level, reaching a maximum value of r= - 0.85 for Austre Broggerbreen and r= -0.74 for Midtre Lovenbreen. This shift in significance between FS ice flux and Svalbard winter climate is contemporary with the shifts in significance between the NAO index and FS ice export (see Figure 7 above).

Summer Mass Balance

In his work on glacier mass balance and climate, Blanchard (2003) showed that during low summer mass balance years (i.e. low ablation) an anomalous northerly airflow is established over the Svalbard area as a result of an area of low pressure over the Kara sea and an intensified Beaufort sea high. Meanwhile, high summer mass balance years (i.e. high ablation) are characterised for an anomalous southerly flow over Svalbard, as an area of high pressure developes over the Beaufort sea. Figure 16 shows the SLP distribution for summers with mass balance in the upper quartile (high summer mass balance), lower quartile (low summer mass balance) and the SLP difference between the composites for Austre Broggerbreen.

i)

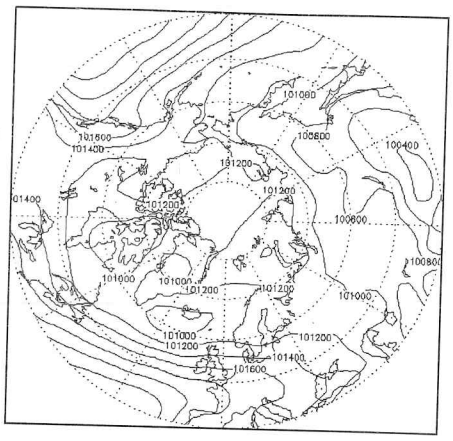

ii)

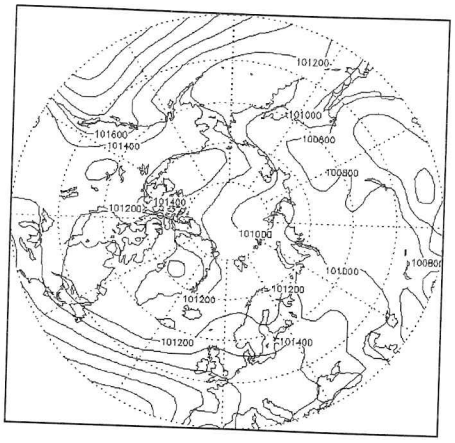

iii)

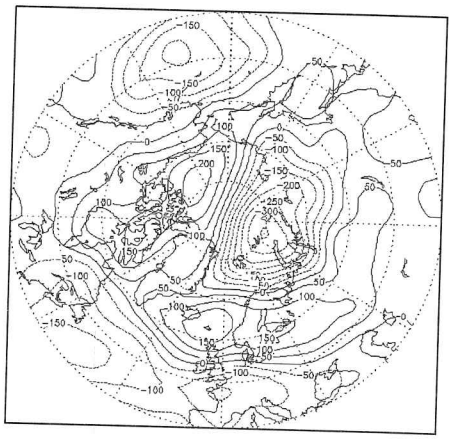

Figure 16. Mean summer (June to August) SLP for i) high summer mass balance, ii) low summer mass balance, iii) difference of composites

Fig 16.c shows clearly the anomalous flow over Svalbard and the FS to be northerly during low ablation years and southerly during high ablation years. We again thus hypothesize that low summer mass balance years are associated with greater than normal summer FS ice flux, whereas high summer mass balance years will also show a decreased summer FS ice flux. Table 9 shows the correlation coefficients between the Häkkinen and Hilmer model results and summer mass balance for Midtre Lovenbreen and Austre Broggerbreen. Several different monthly averages were computed to find the time period that yields the highest correlations.

Table 9

Correlation between model FS ice export and summer mass balance for Svalbard glaciers. JJA = June to August, JAS = July to September, JJ = June to July, JA = July to August, AS = August to September, JJAS = June to September. One asterisk indicates statistical significance at the 5% level, two indicate significance at the 1% level.

	Hilmer FS model output					
	JJA	JAS	JJ	JA	AS	JJAS
Mid.Lov	0,54**	0,40**	0,45**	0,46**	0,31*	0,49**
Aus.Bro.	0,57**	0,45**	0,45**	0,52**	0,33*	0,51**
	Häkkinen FS model output					
	JJA	JAS	JJ	JA	AS	JJAS
Mid.Lov	0,49**	0,51**	0,39*	0,51**	0,41**	0,49**
Aus.Bro.	0,52**	0,54**	0,41**	0,57**	0,41**	0,51**

The highest correlations take place during high summer, June-August period for the Hilmer model, July-August for the Häkkinen model. Lower values at the end of summer (August-September) agree with the end of the Arctic summer towards the end of August.

Figure 17 Summer mass balance and FS ice export for June-July-August. The FS ice export is times by 3 to aide visualisation. Summer mass balance is in units of millimetres of water equivalent.

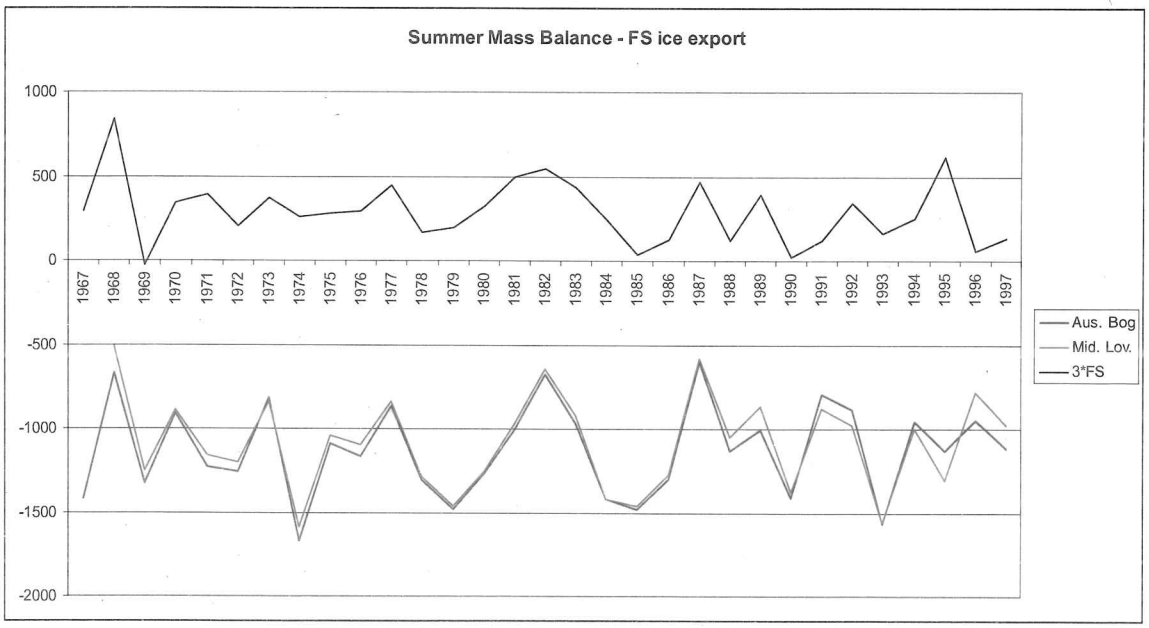

There is a general agreement between FS ice flux and both summer mass balance series throughout the whole period, although at first sight it would appear that there is a loss in correlation towards the end of the period. Figure 18 shows the running 15 year correlation for both glaciers and the corresponding significance levels.

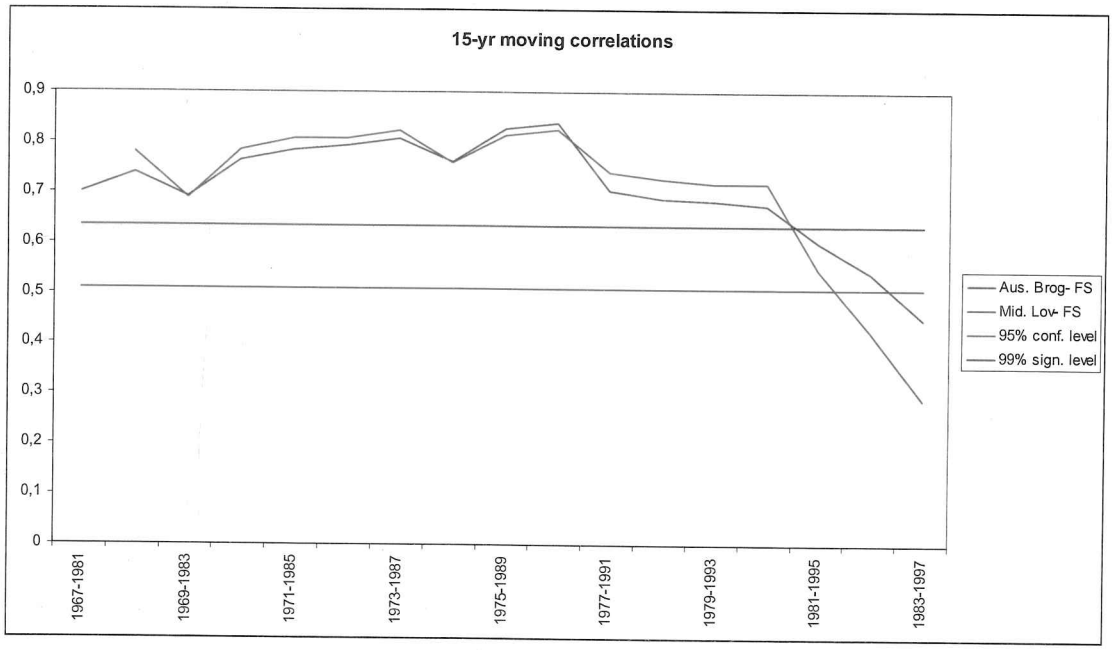

Figure 18. 15 year moving correlations for summer FS ice export and Svalbard summer mass balance

The graph shows clearly a consistent, significant correlation for a majority of the period and decreasing correlation values towards the last few years. It is interesting to note the different behaviour of the FS- Svalbard mountain climate in winter and summer. While winter FS ice flux and Svalbard winter precipitation have shown an increase in correlation over the last two decades, summer FS ice flux and Svalbard summer temperatures show a regular, high correlation for most of the period studied with the exception of the 1990s. The fact that the FS ice flux can be linked to other environmental variables arise the possibility to extend different time series back in time. In this case, the mass balance records for both glaciers may be extended back to 1951, year in which the Häkkinen model runs from. (maybe out: It is

also common in glaciology to obtain net yearly accumulation rates from ice cores thanks to either visible annual layers in the ice core or through the measurement of oxygen isotopes. Ice cores have been obtained from Svalbard (reference here) that have provided net accumulation rates. Since net accumulation rates are the result of winter and summer mass balances as described above, the relationship between FS ice flux and net rate is to be considered.

It is well known that the net mass balance of Arctic glaciers is predominantly driven by the summer mass balance (references here). Table 10 shows correlation values for both Svalbard glaciers.

Table 10

Correlation between measured winter, summer and net balances. One asterisk indicates statistical significance at the 5% level, two indicate significance at the 1% level

Compared variables	Austre Broggerbreen	Midtre Lovenbreen
b_w/b_n	0,40*	0,39*
b_s/b_n	0,86**	0,83**
b_w/b_s	-0,14	0,16

Given the link between summer FS ice flux and Svalbard summer glacier mass balance, it is reasonable to expect some degree of correlation between summer FS ice flux and net Svalbard glacier mass balance (Table 11).

Table 11

Correlations for summer FS ice export and Svalbar net mass balance. One asterisk indicates statistical significance at the 5% level, two indicate significance at the 1% level

	Hilmer FS model output					
	JJA	JAS	JJ	JA	AS	JJAS
ML	0,30	0,25	0,19	0,30	0,23	0,26
AB	0,39*	0,36*	0,24	0,42*	0,30	0,34

Häkkinen FS model output						
	JJA	JAS	JJ	JA	AS	JJAS
ML	0,24	0,34	0,11	0,36*	0,31	0,24
AB	0,31	0,40	0,16	0,45**	0,33	0,29

While most of the correlations are not significant, some values above the 95% confidence level are obtained and one above the 99% level. In spite of this, summer FS ice flux only explains 20% at best of the variability of net glacier mass balance in Svalbard. Thus only approximate estimates of summer FS ice flux may be available from net accumulation rates obtained from Svalbard and vice versa.

Stratosphere - Introduction

The stratosphere is the layer of the Earth´s atmosphere that sits just above the troposphere and below the mesosphere. It is situated at an altitude between 17km and 50 km above the surface at the Equator, while at the poles the boundary between the troposphere and the stratosphere, is located rather lower at around 8 km above the surface. This boundary is called the tropopause. Within the stratosphere, temperature increases as altitude increases; the top of the stratosphere has a temperature of around 270 K. This boundary is called the stratopause and separates the stratosphere from the mesosphere. This vertical temperature stratification, with warmer layers above and cooler layers below, makes the stratosphere dynamically stable; there is no convection and associated turbulence. The warmth of the upper layers of the stratosphere is caused by the ozone layer that absorbs solar ultraviolet radiation (Walter, 2003).

During winter, the circulation in the Northern Hemisphere lower to middle stratosphere is characterized by strong and almost zonally symmetric westerly flow in subpolar latitudes, whereas weaker easterly winds dominate during summer. The winter flow pattern is described as the stratospheric polar vortex. It is mainly thermally driven: as the polar-night approaches, incoming radiation falls drastically leading to the cooling of the northern polar region. The vortex tends to form in early winter and normally decays in late winter / early

spring, when the circulation changes back to the summer situation. However, the vortex may also be subject to disturbances during high winter. Such events are associated with warming of the polar stratosphere, i.e. with a reversal of the meridional temperature gradient, but do not always lead to a change towards easterly winds in the stratosphere, i.e. to a breakdown of the vortex. Such events are called 'Mid-winter warmings'. Warming events that cause vortex breakdowns are named 'Major mid-winter warmings'. In these situations, the centre of the polar vortes is then often displaced to latitudes south of 60-65N or is splitted into several small vortices .

The strength of the winter mean stratospheric polar vortex is characterized by a regime-like behaviour. Studies of probability density (e.g. Christiansen, 2003) have shown that the strength of the stratospheric polar vortex is characterized by two regimes in which the vortex is either primarily strong or weak. There are several ways to measure the strength of the polar vortex. One of the more common ones and that has over recent years gained increased usage is that of mean zonal mean wind speed at 65N and 50hPa geopotential height, that is the height at which there is a pressure of 50hPA, normally around 20km height (Castanheria and Graf, 2003). Using this convention, a mean zonal mean wind speed greater than 20 ms corresponds to a strong vortex, whereas speeds lower than 10 ms are said to correspond to a weak vortex.

Variations in the strength of the stratospheric polar vortex are mainly caused by the interaction of upward propagating planetary waves from the troposphere with the zonal mean flow in the stratosphere (Matsuno, 1970). Other factors can influence the stratospheric polar vortex: Labitzke and van Loon (1988) detected a 10-12 year oscillation in lower stratospheric temperature and geopotential height in phase with the 11 year cycle. Moreover, the Quasi-Biennal Oscillation (QBO) has been shown to have an influence on the probability for a breakdown of the vortex (Labitzke, 1987). The QBO is a near 2 year fluctuation in the direction of the winds in the tropical stratosphere between easterly and westerly flow, with a variable period averaging 28 months (Baldwin et. al, 1994).

From the 1970s to the mid 1990s, the polar vortex strengthened significantly (Perlwitz and Graf, 1995) which led to a cooling of the stratosphere. This change has been linked to an increased concentration of greenhouse gases. This has led to an increase in tropospheric temperatures in lower latitudes, which produces an intensification of the polar winter vortex as the geopotential layers in the tropics increase in height, producing a greater pole-tropic gradient and thus a strengthening of the vortex. This strengthened vortex then causes polar cooling because the transport of heat to polar latitudes by planetary waves is reduced and air parcels inside the vortex are more confined to the polar latitudes, thus remain in shadow during greater times thereby cooling toward the radiation equilibrium.

Figure 19 Strength of the stratospheric polar vortex for i) all winter months (December to March) and ii) mean winter values from December 1958 to March 2004 (The year on the x-axis refers to the year in which January falls for that particular winter).

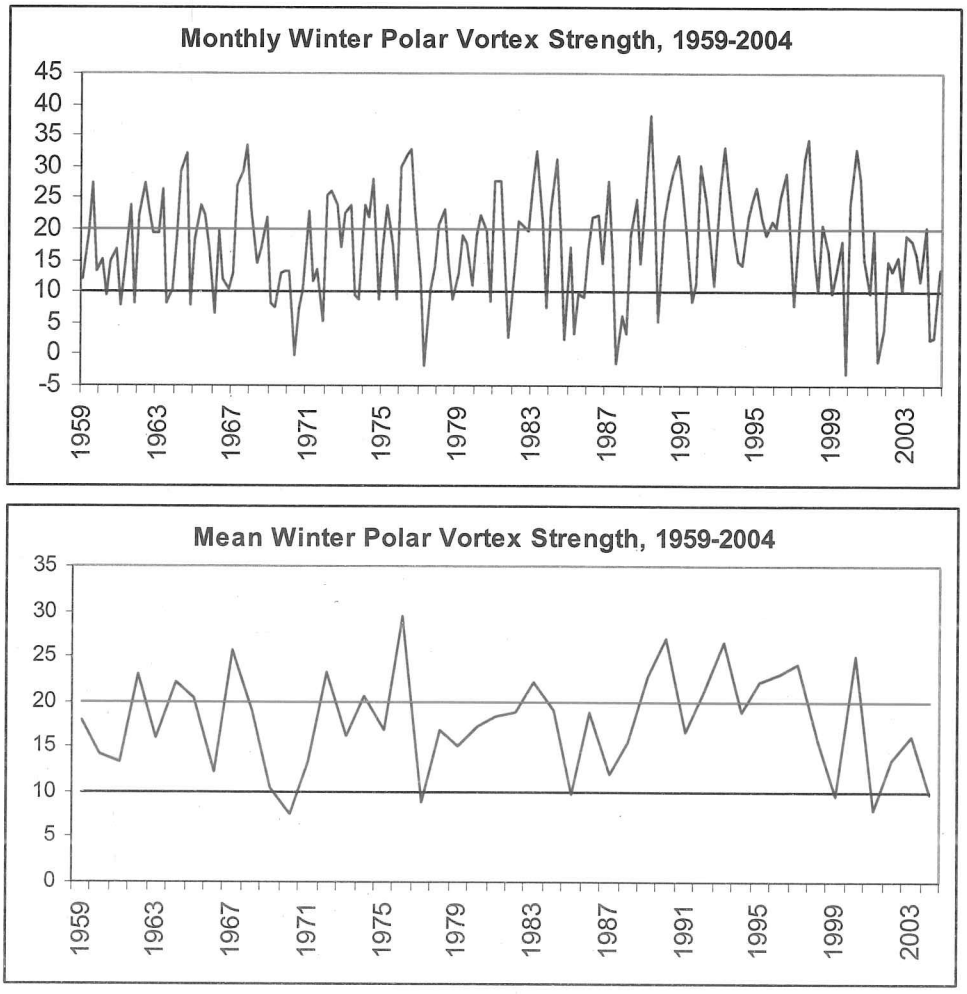

While they both show the mentioned increase in vortex strength towards the end of the 1990s which has been linked to anthopogenic global warming, it is also clear that the vortex has undergone a marked weakening within the last 5-7 years. Considering that 3 of the 4 warmest years globally have occurred in this period (2002, 2003, 2004), this is not compatible with the notion of a straitghtforward increase in vortex strength associated with warming tropospheric temperatures. Both graphs show the limits (10 and 20ms) for classification of strong and weak vortex regimes. There are 74 months of strong vortex regime and 39 months of weak vortex regime.

Stratosphere – Troposphere coupling

Until relatively recently, it was commonly believed that the stratosphere had little influence on the state of the troposphere, and that it was merely a passive recipient of energy and waves from the troposphere below it (e.g. Baldwin et al, 2003). Statistical studies in the last decade have shown that the stratosphere may modulate low frequency atmospheric variability in the troposphere. Baldwin and Dunkerton (1999) presented evidence for the downwards propagation of geopotential anomalies from the stratosphere to the troposphere, and found a mid-winter correlation exceeding 0.65 between the 90-day low-pass-filtered 10hPa (~30km) anomaly and the 1000hPa (surface level) anomaly when the surface anomaly time series was lagged by about three weeks. Later work (Baldwin and Dunkerton, 2001) has shown that the largest stratospheric anomalies originate above 1hPa and descend through the stratosphere within 1-2 weeks. In general, only the strongest anomalies of either sign appear to connect to the surface, whereas weaker anomalies typically remain within the stratosphere. Hence, tropospheric high frequency variability seems to be unconnected to the stratosphere. There are two mechanisms by which the stratosphere is thought to influence the troposphere. Hartley et al. (1998) propose that large-scale anomalies of potential vorticity in the lower stratosphere induce a geopotential anomaly in the polar troposphere through hydrostatic and geostrophic adjustment of the atmospheric column. A strong polar vortex is thus associated

with anomalously low pressure in the troposphere near the pole. This process can be pictured as a large-scale annular stirring of the troposphere from above. The second mechanism involves the interaction of planetary waves in the troposphere with the mean flow in the lower stratosphere (Matsuno, 1970). Zonal winds in the stratosphere influence the refractive index of upward propagating waves- when the zonal mean zonal wind in the stratosphere exceeds a critical velocity, planetary waves that are propagating upwards from the stratosphere are reflected back downward and in meridional direction. Once reflected, these waves can interfere either constructively or destructively with the tropospheric wave pattern. Thus the stratosphere acts on the troposphere only if the polar vortex is strong (Perlwitz and Graf, 2001).

For the purpose of this thesis, it is necessary to consider the stratosphere and its influence on the troposphere in terms of the influence on the relevant modes of atmospheric variability in the North Atlantic region the stratosphere may have. In other words, how does the stratospheric polar vortex influence the North Atlantic Oscillation and does the state of the vortex in terms of strong or weak regimes influence the mode of variability in the region. Baldwin and Dunkerton (2001) show that a strong (weak) stratospheric polar vortex tends to be associated with a positive (negative) NAO index phase in the troposphere, such that during the weak vortex regime, the average value of the AO index is -0.44, and +0.35 for strong vortex regimes. These results agree with the above notion that a strong vortex in the stratosphere will lead to a lowering of SLP at the poles, which is associated with a positive phase AO (and thus generally speaking NAO). Perhaps more relevant to tropospheric variability than the shift in the means are the differences in the shapes of the probability density functions of the AO and NAO indices during weak and strong vortex regimes. Values greater than 1.0 (lower than -1.0) of the normalized indices are 3 to 4 times as likely during strong (weak) vortex regimes than weak (strong) vortex regimes. Values exceeding these thresholds (+1.0 and -1.0) of the AO index are associated with an increase in the probability of extreme winter weather phenomena such as large winter storms or cold air outbreaks over

large parts of Europe and eastern North America. The storm track in the North Atlantic is also shown to be significantly displaced southward during weak vortex regimes, especially over the eastern North Atlantic and downstream over Europe.

More recently, Graf and Walter (2005) have shown that the upper troposphere teleconnections patterns that arise in the North Atlantic region differ greatly between vortex regimes. During the strong vortex regime, one teleconnection pattern emerges (NA-SVR in the following) of two zonally elongated areas of strong teleconnectivity over much of the North Atlantic (figure 20, left). Their centres are over southwest Greenland and the subtropical central North Atlantic. During the weak vortex regime, two teleconnections patterns, mostly independent of each other, are present, one over the eastern North Atlantic and the other over the western North Atlantic (Figure 20, right, eastern NA-WVR and western NA-WVR in the following). The former has centres of action northwest of Iceland / east of Greenland and west of Iberia, while the latter is found with centres of action over northeastern Canada and the western subtropical North Atlantic (Figure 20, right).

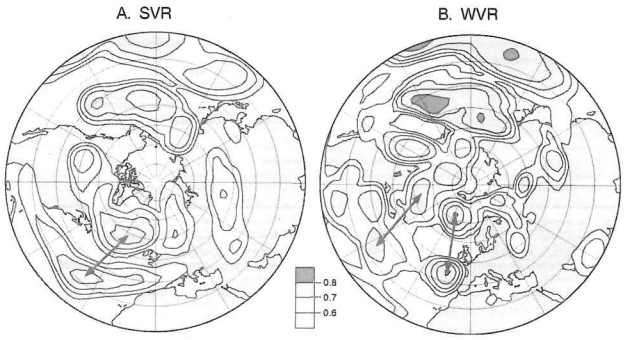

Figure 20. Teleconnectivity for monthly mean 300 hPa geopotential height for i) strong polar vortex regime and ii) weak polar vortex regime. Arrows indicate location of teleconnections.

We construct index time series for all three patterns using the difference of normalized 300 hPa geopotential height anomalies at the southern and northern centres of action of each teleconnection pattern: 65-70N, 27.5-35W and 37.5-40N, 15-22.5W for the eastern NA-WVR; 62.5-65N, 77.5-82.5W for the western NA-WVR; and 55-60N, 30-45W and 30-35N, 35-45W for the NA-SVR (Figure 21).

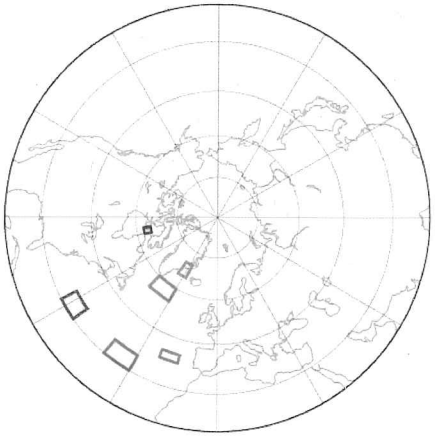

Figure 21. Geographical location of areas for the computation of teleconnection patterns: red) eastern NA-WVR, black) western NA-WVR and blue) NA-SVR

The different polarities of these modes show significant anomalous 850 hPa wind fields over large areas of the North Atlantic, and thus anomalous temperature and precipitation patterns (Figure 21).

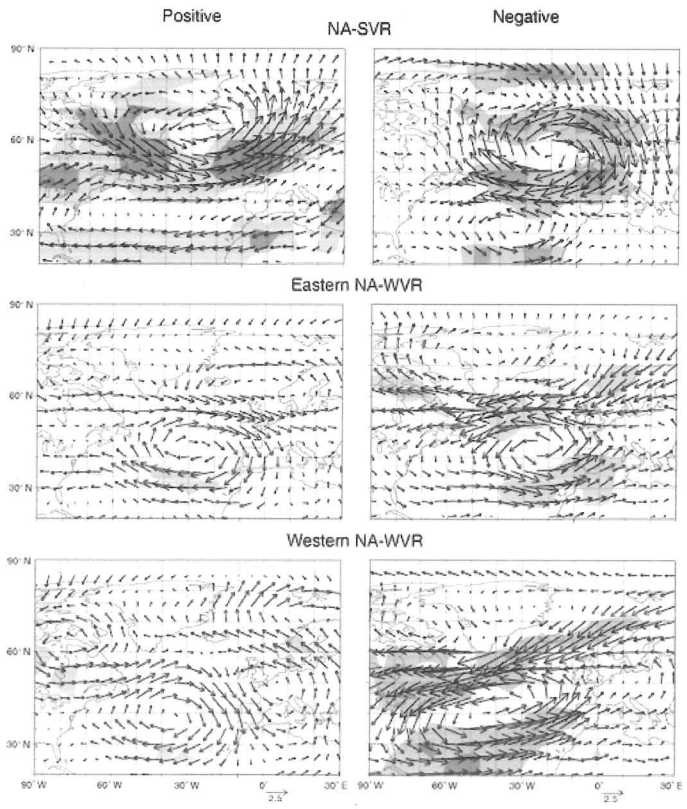

Figure 21. Composite anomalies for 850 hPa wind anomaly (from 1958-1998 mean) for the positive (left) and negative (right) phase. Shadings indicate anomalies above the 95% (light) and 99% (dark) significance level.

During the strong vortex regime, circulation varies from strong cyclonic in the positive phase (deep Icelandic low) to anticyclonic in the negative phase (blocking high over the northeast Atlantic). When the polar vortex is weak, both teleconnections are mainly associated with the wind field of the subtropical (Azores) high. These vortex-strength depending teleconnections patterns are not present at sea level (Walter and Graf, 2005). However, storm tracks, and the associated precipitation, are dependant on middle and upper tropospheric conditions rather than surface conditions. In addition, the high surface winds and wave action associated with these mid-to-high-latitude storms have a significant impact on sea ice conditions (see below). Perhaps the most revealing result of the work of Graf and Walter (2005) is the finding that the negative phase of the teleconnection pattern during the strong polar vortex regime corresponds to an atmospheric mode not captured by the classic NAO index. It corresponds to a blocking situation over the North Atlantic with a very strong northeastward tilt of the storm track axis and reduced precipitation over Western Europe. In other words, a stationary area of high pressure south of Iceland and west of the British Isles forces North Atlantic storms to circle it along its northern edge, pass the Davis Strait and then westward towards Scandinavia.

Polar vortex strength and FS ice export.

The link between the stratospheric polar vortex and FS ice export is investigated by computing the correlation between the two variables (see table 12).

Table 12

Correlation between winter (DJFM) stratospheric polar vortex strength and FS ice export for lags varying from 0 to 4 months.

Lag (months)	Widell	Häkkinen	Hilmer
0	0,14	-0,01	0,04
1	0,27	0,03	0,06
2	0,21	0,03	0,07
3	0,17	0,00	-0,01
4	-0,10	0,02	-0,00

There is no significant correlation between the two variables, although it is tempting to suggest that the higher value at 1 month lag for the observational data corresponds to Baldwin and Dunkerton (2001) findings that stratospheric disturbances take on average 3 weeks to reach the troposphere. This value (r=0,27) is significant at the 10% level. This result is compatible with two facts: i) that a strong (weak) polar vortex is associated with a positive (negative) index NAO, and ii) that during the 1990s, there was a significant positive correlation between the NAO index and FS ice export (see Figure 7 above). Thus, at least during the 1990s, one would expect a small but significant correlation between the stratospheric polar vortex and FS ice export. Both model data show no correlation between stratospheric polar vortex and FS ice export. This may result from the lack of significant NAO – FS ice export correlation for the whole period (see table 3 above).

Upper troposphere teleconnection patterns and FS ice export.

Graf and Walter (2005) show that depending on the state of the vortex and the polarity of the upper troposphere teleconnection pattern different low troposphere wind anomalies over the North Atlantic and adjacent land areas are set up (Figure 21). In the vicinity of the Fram Strait, during strong vortex episodes, an anomalous southerly (northerly) 850hPa wind anomaly is associated with a positive (negative) phase of the teleconnection pattern index. The anomalous 850hPa wind field over the Fram Strait is statistically significant at the 99% level for the negative polarity of the teleconnection pattern, but is not significant to the 95% level for the positive phase. During weak vortex episodes, there is little difference between the 850hPa wind field in the Fram Strait between the polarities of the teleconnection patterns, and no significant differences arise. If one assumes that the wind field at surface level will be to a large extent in phase with the wind field at 850 hPa (which is around 1.4 km above sea level at high latitudes), it is thus to be expected that during strong polar vortex episodes, there will be a negative correlation between the 300hPa index and FS ice export, while during weak vortex episodes, no correlation is expected between the two variables. Table 13

shows the correlation values between the modelled FS ice export data, the 300hPa index data and the NAO index for months with strong and weak polar vortex.

Table 13

Correlation coefficients for teleconnection patterns indexes and FS ice export. nH refers to the numbers of months of strong and weak vortex regimes during December to March for 1958-2000, nHi for 1958-1997. One asterisk indicates statistical significance at the 5% level.

	nH	nHi	Häkkinen	Hilmer		Häkkinen	Hilmer
NA-SVR	74	70	-0,18*	-0,12	NAO	-0,08	-0,01
Eastern NA-WVR	36	32	0,21	0,32*	NAO	0,10	0,22
Western NA-WVR			0,00	0,08			

During strong vortex episodes, these results agree with the above hypothesis. However the correlation values are low and only Häkkinen´s data is significant to the 5% level. It is nevertheless noteworthy that an index constructed out of 300hPa geopotential anomalies shows significant correlation while the NAO index which is constructed out of SLP anomalies and has its centres of action closer in distance to the Fram Strait does not show any significant correlation. During weak vortex regimes, one statistically significant result arises, a positive correlation between the Eastern NA-WVR index and Hilmer FS ice export. This disagrees with expectations that no significant correlations would be found. However, the positive correlation agrees with wind anomaly directions in Figure 21 and may result from the closer proximity to Fram Strait of the centres of action. Results of the above analysis with observational data of FS ice flux was not included, as the number of winter months during 1990-1999 with a strong or weak vortex was deemed to low for any meaningful analysis.

Atmosphere – Sea ice interaction

Variations of sea ice have received increased attention recently in the context of possible associations with anthropogenic climate change. The evidence from the past 2-3 decades indeed points to a decrease of ice coverage in the Arctic (e.g. Chapman and Walsh, 1993; Parkinson et al, 1999). Sea ice fluctuations are driven by atmospheric and oceanic variability. As with sea surface temperatures (SSTs), the frequency of sea ice variability is lower than that for air temperature owing to its higher heat capacity and slower transport velocity. As with the Fram Strait ice flux, sea ice coverage has been rendered to be highly important to the Earth's climate system, due to its influence on global albedo, heat exchange control between the atmosphere and oceans and on ocean currents. In this section of this work I will be reviewing the sea ice fluctuations in the zone between the Arctic and the North Atlantic. The areas are selected in terms of annual variability patterns within the Barents, Nordic Seas and the Labrador seas. Other seas in the area in which winter sea ice is present, such as the Gulf of St Lawrence or the Baltic sea are ignored due to their insularity with respect to the North Atlantic.

General sea ice patterns

Figure 22 shows the mean monthly sea ice extent (left) and variability (right) for October 1978 to June 2001. The variability is expressed in percentage variance (see colour bar).

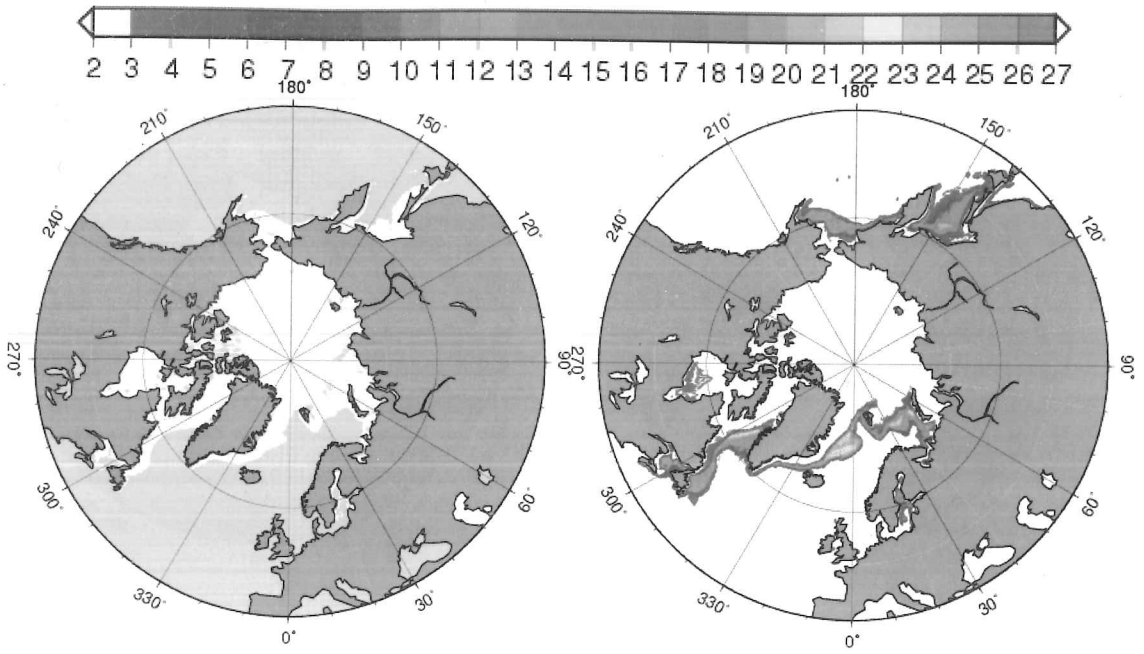

1) January

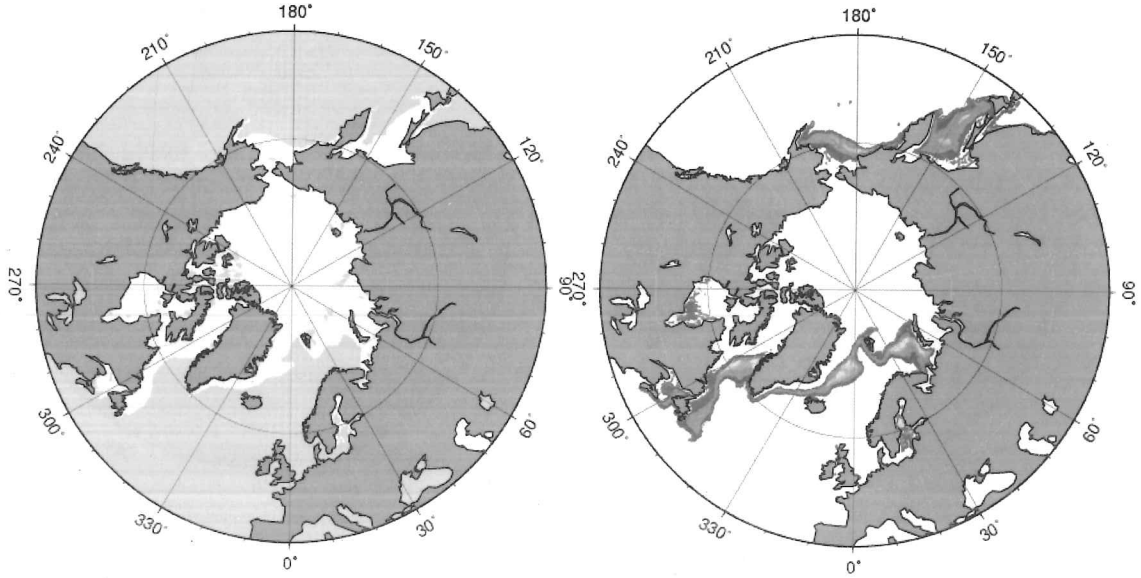

2) February, and 3) March, below.

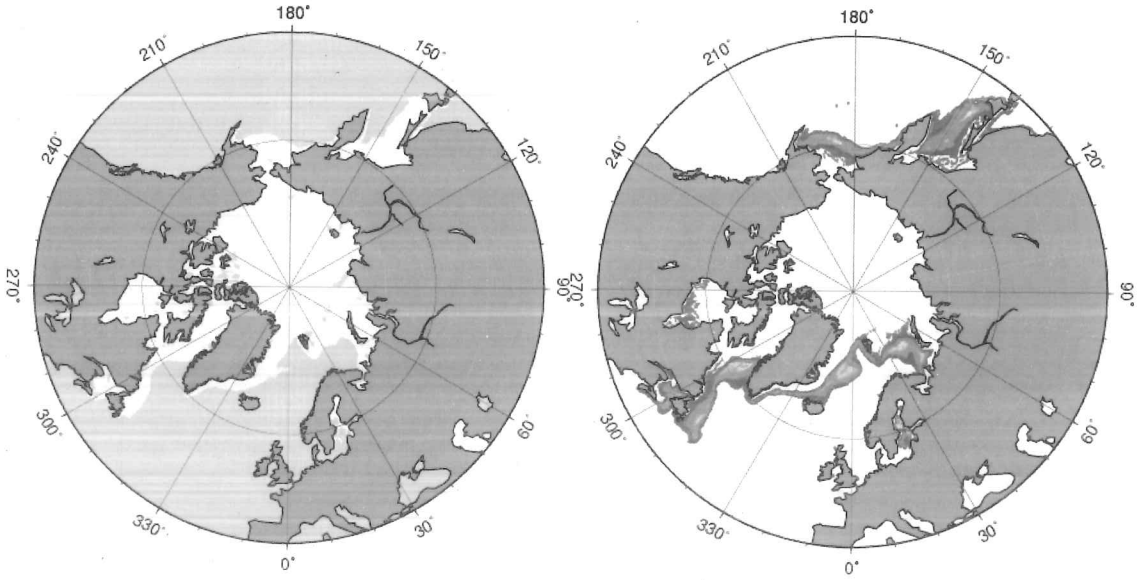

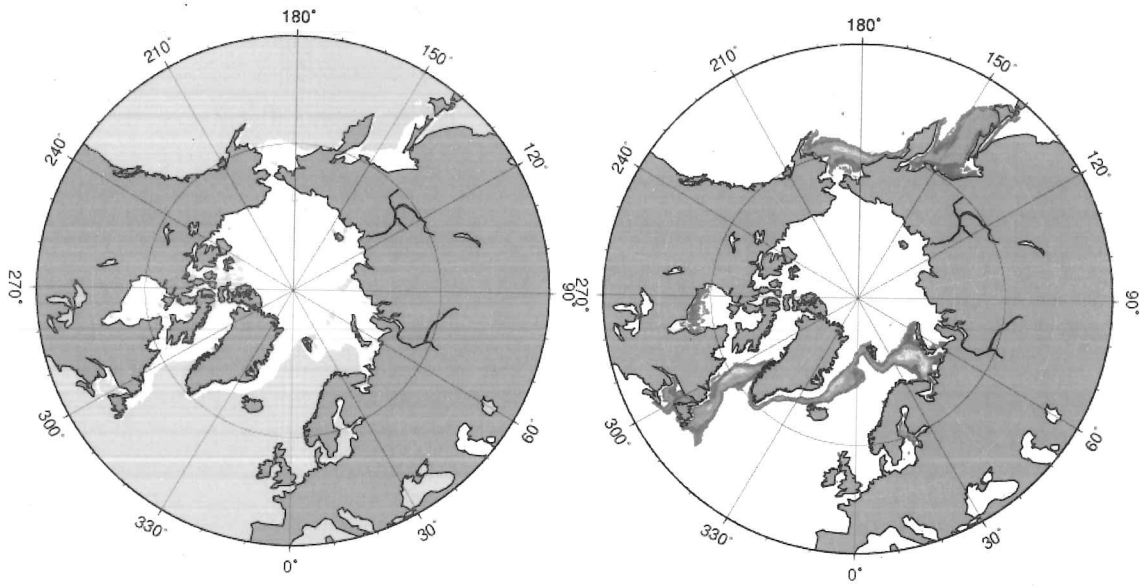

4) April

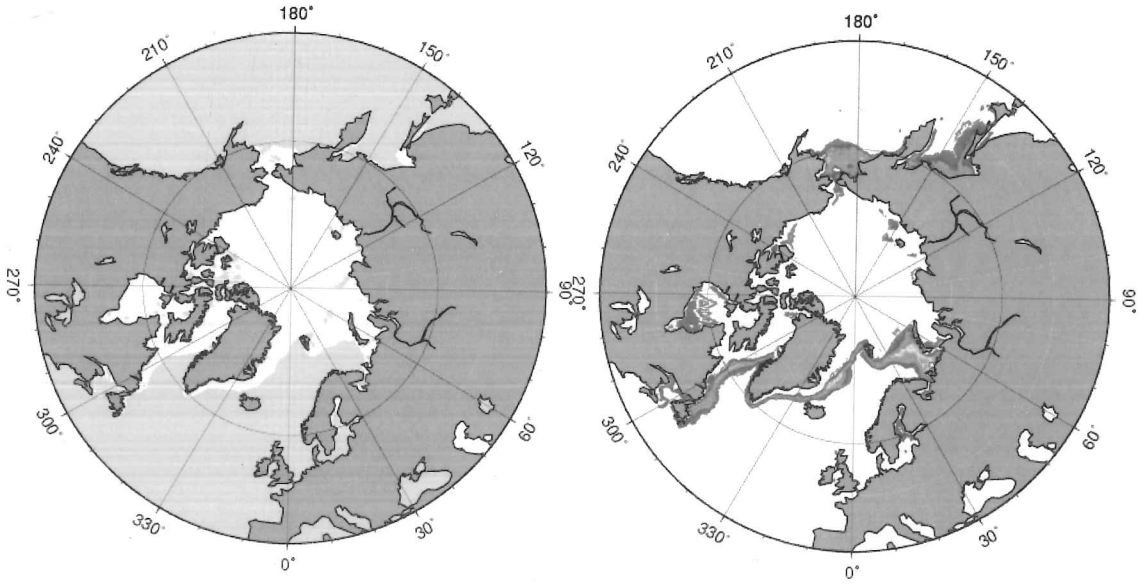

5) May

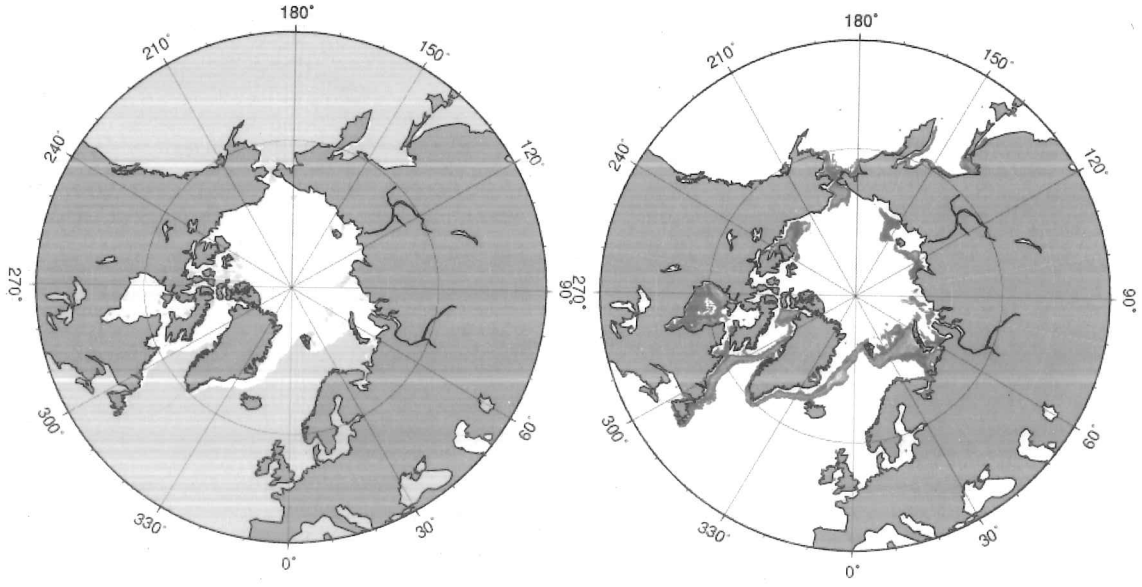

6) June

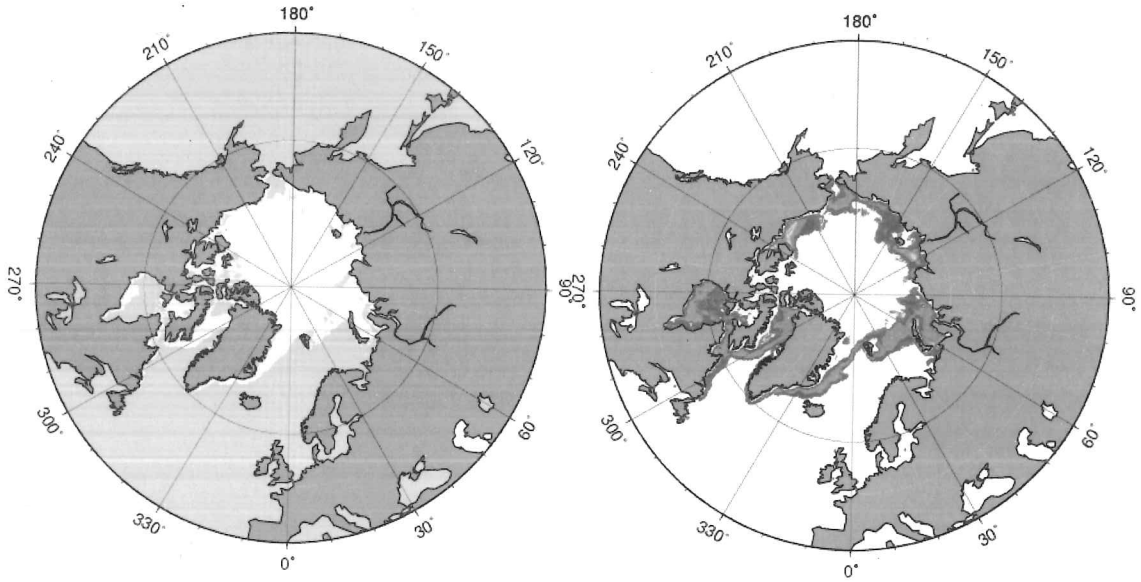

7) July

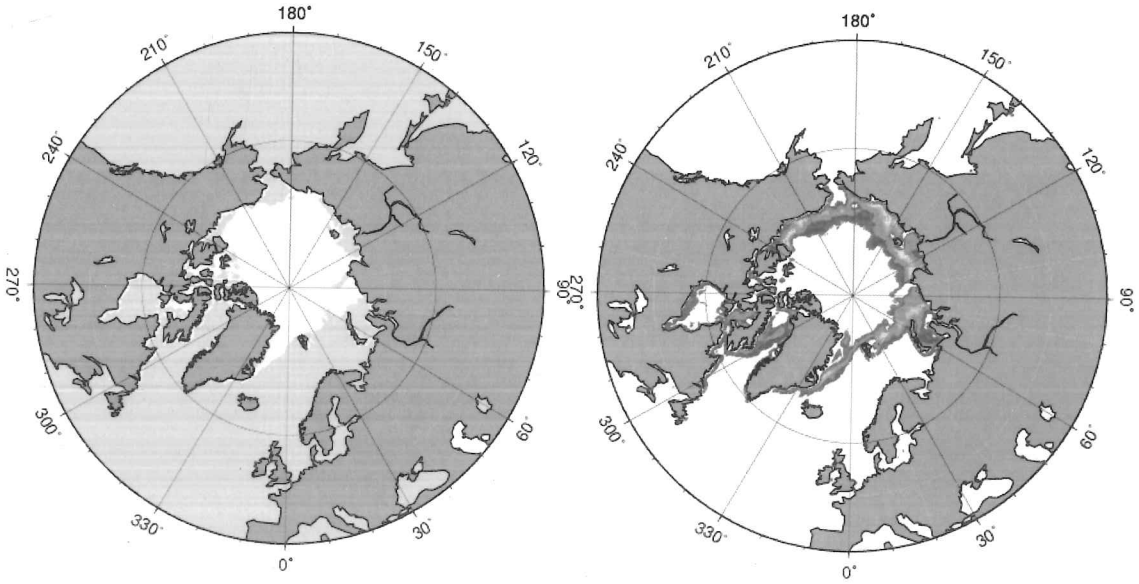

8) August

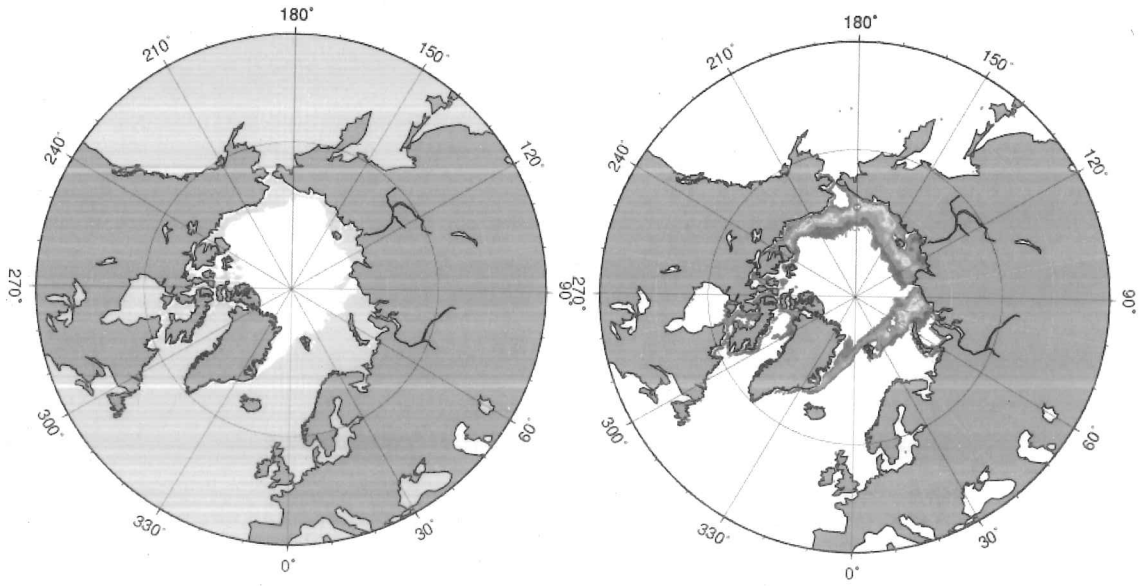

9) September

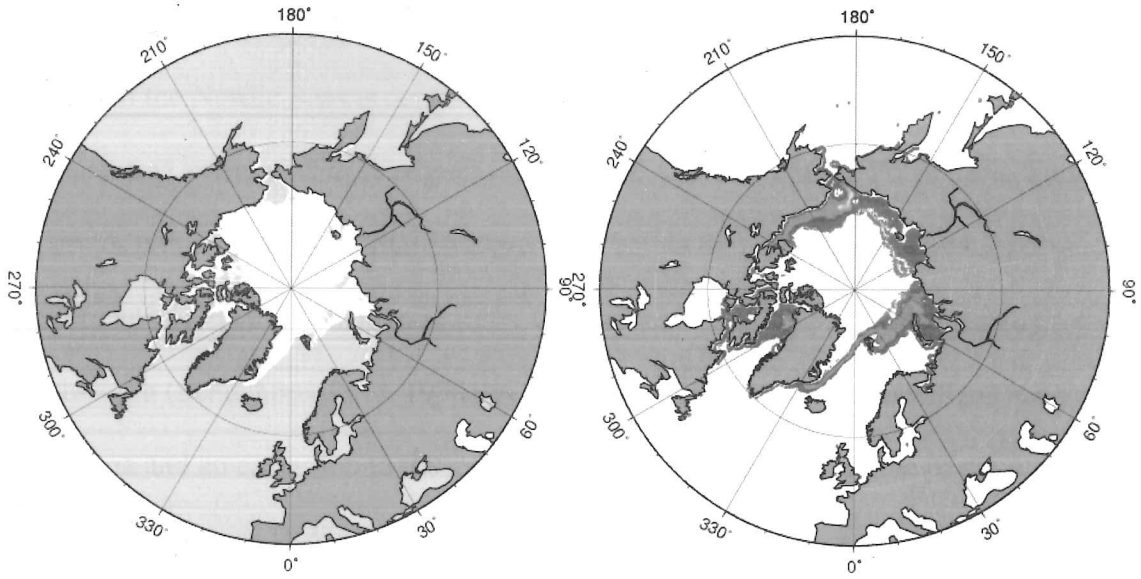

10) October

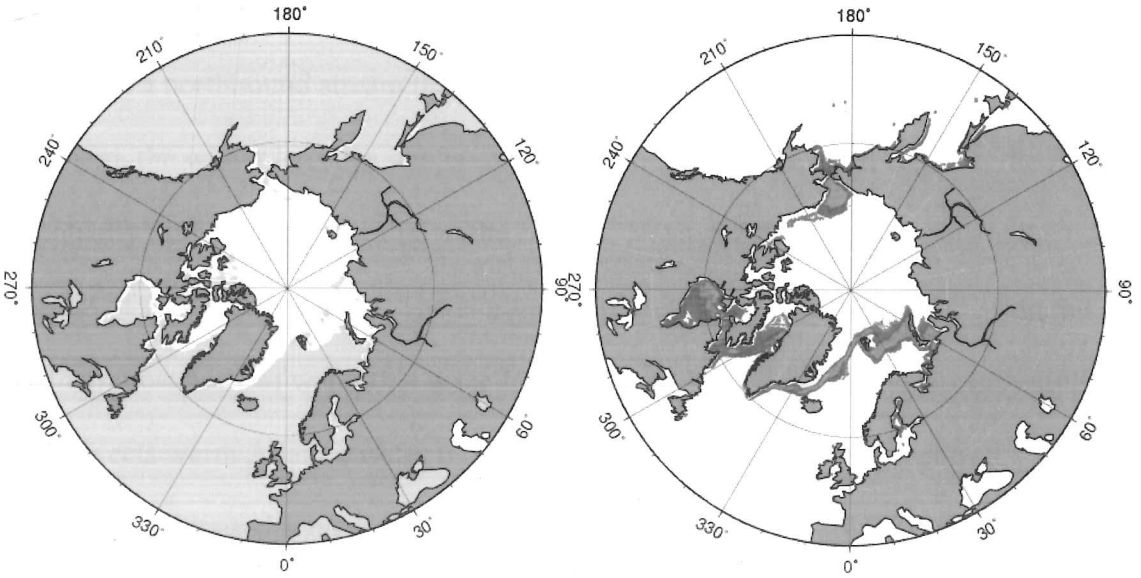

11) November

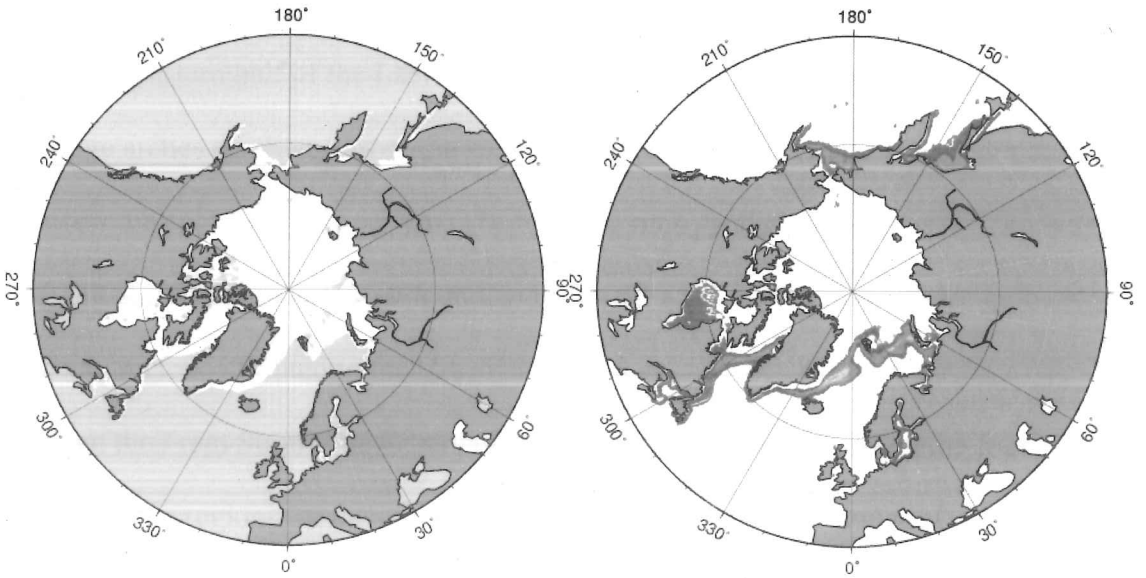

12) December

Sea ice in the Nordic Seas is confined to the eastern coast of Greenland where during winter the eastward extent of the ice edge is limited by the location of the Polar front. This front separates polar water in the EGC (temperature below 0C and salinity below 34.5 practical salinity units or psu) from atlantic water types (T>2C, S>34.9 psu) and generally trends north-south (Schuchman et al, 1998). A conspicuous feature in the Greenland sea ice panorama and an exception to the general north-south trend is a tongue of sea ice that just out of the ice edge near 10W called the Odden at around 72-74N (Schuchman et al, 1998). Around the Fram strait area the ice edge envelopes around Svalbard, and is of different provenance than ice in the Greenland sea: along the western coast of Svalbard, the ice is present in a northbound stream that emerges from the Barents sea (Vinje, 2001). Southeast of Svalbard, the winter ice edge wraps around the northern and eastern edges of the Barents sea eventually running south parallel to the coast of Novaya Zemlya and ending at the eastern portion of the Kola peninsula. The Norwegian-Barents region is unique for being the northernmost body of water that is ice free in winter. This is due to the North Atlantic drift that advects warm Atlantic water types into the area. Once the EGC reaches the southern tip of Greenland, it carries on along the Greenland west coast as the West Greenland current. Along the southwest coast of Greenland warmer Atlantic waters are advected northward along with the cold polar waters from the EGC, resulting in a much reduced sea ice extent, while the eastern half of the Labrador sea remains ice free to around 65N north. Here the sea ice edge arches southwest from the west Greenland coast towards the Labrador coast, where it meets the cold Labrador current. The ice edge runs parallel to the coast of Labrador some 200-300 km wide towards Newfoundland where it ends. In summer, sea ice in the North Atlantic region is limited to the Greenland sea, that is advected from the Arctic ocean through the Fram Strait. The Greenland sea is thus rather unique within the frame of Arctic and subarctic regions for having one of the lowest seasonal amplitudes of sea ice extent change (Mysak and Manak, 1989, see Figure 22 above). It is clear that ocean circulation is

the main forcing agent of sea ice location. In the Arctic / North Atlantic region, there are four main areas of variability: the Barents sea, the Greenland Sea, the northern Labrador Sea and the southern Labrador Sea. The following part of this work focuses on sea ice variations in these regions, together with southeastern Greenland which provides the link between the Greenland Sea – Barents Sea and the Labrador Sea. The boxing of the Greenland and Barents seas follow the convention in Vinje (2001). The selected areas are shown in Figure 23.

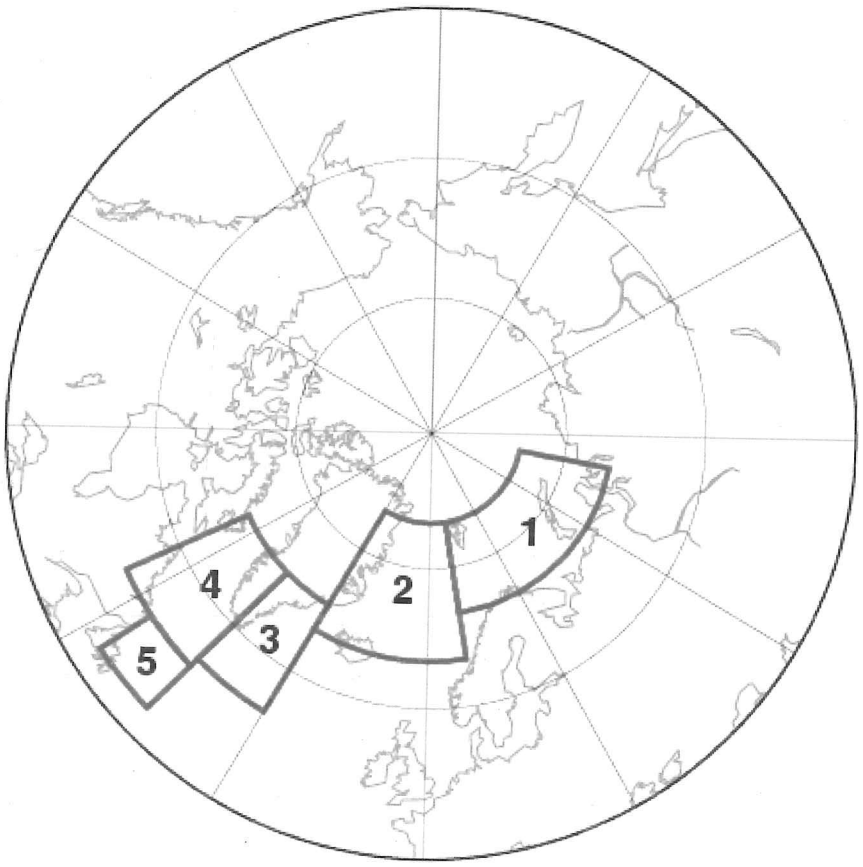

Figure 23. Selected sea ice areas: 1= Barents Sea, 2=Greenland Sea, 3= Southeast Greenland, 4= northern Labrador Sea, 5, southern Labrador Sea.

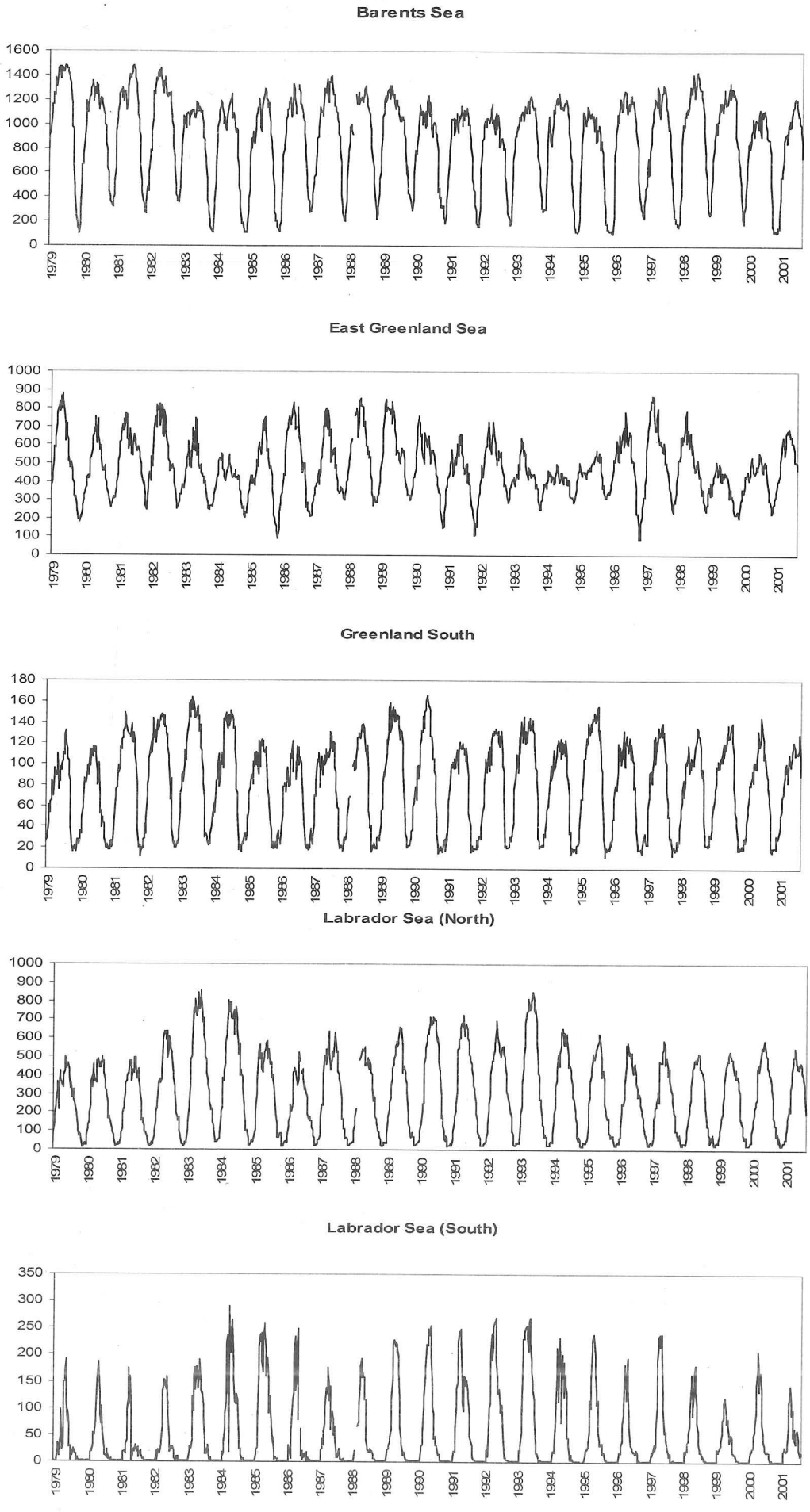

Figure 24 shows sea ice extent in thousands of km2 for all five areas.

All areas show marked seasonal fluctuations. The Greenland, Barents, and southeast Greenland seas maintain some sea ice throughout the summer- the minimal summer sea ice observed in the northern Labrador sea and south east Greenland sea is spurious, resulting from a 'spillage effect' of the satellite brightness temperature signal, a common defect in satellite observations where coastal pixels appear as sea ice rather than open ocean (Parkinson et al, 1999). The Barents and Greenland seas annual cycles are associated with short lived minima at the end of summer and a broad maximum during the late winter months. It is clearly seen how the Greenland sea has a low seasonal variation, with summer ice extent just under half that of winter, but has a very high winter variation, with some years such as 1994, 1995 showing only a slight increase over the summer ice extent and being half the area of winters with large ice extent such as 1979. The Greenland sea and Barents seas ice cover are in phase with one another, showing a marked 8-10 year oscillation. Overall both sea ice areas show a decrease over the 23 year period. The 'south Greenland' region comprises the southern portion of Greenlands east coast, where the EGC is joined by the warm Atlantic water type Irminger current. The sea ice here is advected within the EGC rather than locally formed. It can be seen in fig. xy that for the first half of the period it has a cycle that closely follows that for the Greenland sea but with a lag of about 1-2 years. However, in the last 10 years it has not undergone significant fluctuations and bears little relationship with the last 10 years of Greenland Sea extent. Over the whole period, there is no sign of a significant positive or negative trend in sea ice extent. The northern Labrador sea has a marked 10 year cycle which is out of phase with that for the Barents and Greenland seas cycles. The southern Labrador sea is lagged 1 year with respect to the northern Labrador until the last 5 years when record minimum ice extent takes place. The seasonal maximum extent is used to look at interannual sea ice extent variability; where appropriate integrated sea ice extent over a discrete time period is used. Figure 25 shows the winter maxima for all 5 areas.

Figure 25. Yearly winter maxima for all 5 areas.

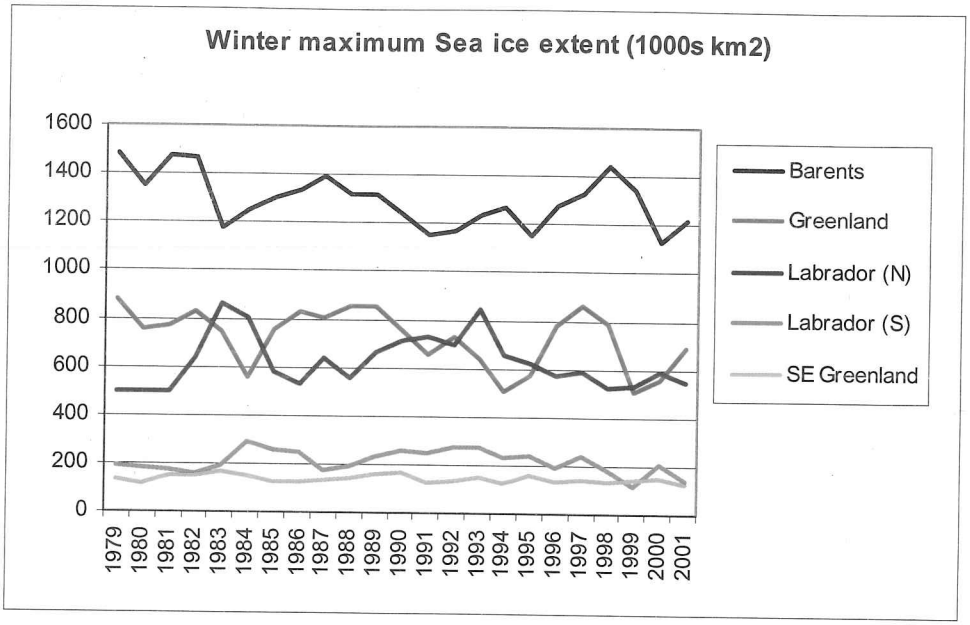

It shows rather well the general patterns between the different areas discussed above. Table 15 shows the correlation matrix between all five areas with zero lag.

Table 15

Correlation coefficients for winter sea ice maxima for all 5 sea areas studied. One asterisk indicates statistical significance at the 5% level, two indicate significance at the 1% level

	Greenland	Labrador north	Labrador south	S. E. Greenland
Barents	0,56**	-0,55**	-0,46*	-0,15
Greenland		-0,29	-0,12	-0,03
Labrador north			0,55**	0,49**
Labrador south				0,13

The Barents and northern Labrador seas yield the most significant correlations, and can thus be thought of as the centres of action of a sea-ice dipole, in which generally speaking positive (negative) anomalies in the Barents- Greenland seas will be associated with negative (positive) anomalies in the Labrador sea. S.E. Greenland stands out as the more independent region, being solely correlated with Labrador (north). Some interesting results arise. While a priori one would expect rather high correlations between Labrador (south) and Labrador

(north), the signal in the Labrador N explains as much of the variance of the Barents sea as it does of the Labrador south, 30% (R=0.30). This perhaps reflects the location of southern Labrador in the mean storm track of the North Atlantic during winter, and thus the sea ice extent area may be very sensitive to the exact location of the storm track. This is because a shift of just a couple degrees north or south of the storm track would affect the location of warm sectors embedded in the cyclones, and thus the climatic conditions over the southern Labrador sea. Sea ice conditions in south east Greenland also appear largely independent to the other seas, apart from the northern Labrador sea.

Temporal relationships.

Table 16 shows the results for the lagged correlations for winter maxima for adjacent regions, and following the direction a parcel of water would follow (thus from regions 2-3-4-5 in Figure 23, the Barents and Greenland seas are poorly connected in terms of ocean currents). The most significant result is the high correlation values obtained for Labrador North-South for 1 and 2 years. The general patterns of lagged correlations reflects the travel path and time of sea ice and SST anomalies in the North Atlantic /Arctic system described by others (e.g. Mysak and Manak, 1989; Venegas and Mysak, 2000). The Barents and Greenland seas react to the same climatic forcing simultaneously, and there is little link between the two areas in terms of ocean transport. Thus no significant lag correlations appear, either for Barents leading Greenland or viceversa (results not shown). The Greenland and S.E. Greenland seas are poorly connected, despite the majority of S. E. Greenland sea ice being advected from the Greenland sea via the EGC. The correlation only becomes significant for a 2 year lag, which agrees with the travel time for ice in the EGC to reach south east Greenland (Mysak and Venegas, 1998)

Table 16.

Correlation coefficients for lagged winter sea ice maxima. One asterisk indicates statistical significance at the 5% level, two indicate significance at the 1% level				
Lag (years)	Barents-Greenland	Greenland - S.E. Greenland	S.E. Greenland- Labrador north	Labrador north - Labrador south
0	0,56**	-0,13	0,54**	0,55**
1	0,23	0,18	0,43**	0,71**
2	-0,02	0,37*	0,12	0,63**
3	0,09	0,17	-0,02	0,19
4	0,22	0,02	-0,19	-0,24

Summer sea ice variability

Summer sea ice extent is significant in the Greenland sea and the Barents seas. Although both the south Greenland and Labrador (north) show a summer sea ice area of around 20 thousand km2, this is a result of 'spillage effect'. Summer sea ice in the Greenland and Barents seas follow very different trends. In the Barents sea, winters with large (low) sea ice extents tend to be followed by summers with large (low) sea ice extents. In the Greenland sea, there is no clear pattern.

Figure 26 Yearly summer maxima for both regions with the previous winter sea ice maxima.

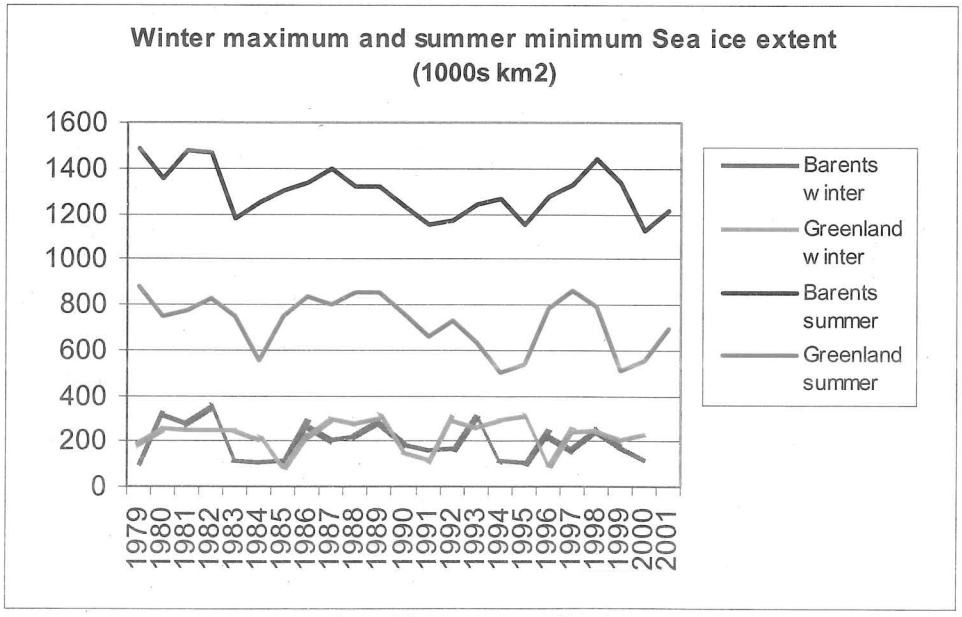

The summer sea ice minima do not show any significant trends as opposed to the winter maxima. As opposed to winter, there is overall little agreement between both regions in the summer sea ice extent, with no significant trends. Table 17 shows the correlation values for the series.

Table 17

Correlation coefficients for summer sea ice minima and winter maxima. "winter-summer" indicates the winter leads the summer and vice-versa. One asterisk indicates statistical significance at the 5% level, two indicate significance at the 1% level

Barents winter-summer	Greenland winter-summer	Barents-Greenland summer
0,50**	-0,06	0,20
Barents summer-winter	Greenland summer-winter	
0,24	-0,19	

As table 17 shows, there is no significant correlation between the summer sea ice minima for the two regions. In the Barents sea, summer sea ice minima is significantly correlated with the previous winter sea ice maxima, but does not influence significantly the next winter maximum. In the Greenland sea, there is no correlation between summer and winter ice values. This is hypothesised to reflect the different sea ice regimes in the two areas. In the Barents area, both winter and summer ice is of thermodynamical origin (it is not advected from elsewhere), and thus how much winter sea ice is produced will have an effect on how much ice is present in the following months.

In the Greenland sea, winter sea ice variability is mainly driven thermodynamically by sea ice formation and melting in the Odden region (Wadhams and Comiso, 1999), whereas summer sea ice extent is presumed to be driven by advection of Arctic multiyear ice through the Fram Strait. To test this, correlations were calculated for Greenland summer sea ice

extent minima and FS ice export values for the previous winter and the same summer. Only the highest values obtained are shown (several monthly combinations were computed to find the optimal time period).

Table 18

Correlation coefficients for Greenland sea summer sea ice minima and Fram Strait ice export during the previous winter and the same summer. One asterisk indicates statistical significance at the 5% level, two indicate significance at the 1% level

	Hilmer	Häkkinen	Widell	Hilmer	Häkkinen	Widell
	January-February-March			June-July-August		
Greenland sea Summer min.	0,57**	0,48**	0,80**	0,71**	0,62**	0,67*

There is a significant correlation between both winter FS ice export and the following summer ice extent in the Greenland sea and the simultaneous summer FS ice export and Greenland. While this may seem slightly contradictory at first, the logical explanation is that winter FS ice export controls how much ice is advected to the Greenland sea, while the climatic conditions that lead to a high (low) summer FS export, in other words enhanced northerly (southerly) flow, are at the same time responsible for anomalously cold or warm summer temperatures in the Greenland sea region. The same analysis was performed for the Greenland sea winter sea ice maxima. The results are shown in table 19- only the months with highest values are shown.

Table 19

Correlation coefficients for Greenland sea winter sea ice maxima and Fram Strait ice export during the previous summer and the same winter. One asterisk indicates statistical significance at the 5% level, two indicate significance at the 1% level

	Hilmer	Häkkinen	Widell	Hilmer	Häkkinen		Widell	
	DJF	DJFM	DJF	AS	JJ	AS	JJA	AS
Greenland sea Winter max	-0,42*	-0,21	-0,37	-0,07	-0,18	-0,03	-0,25	0,17
Greenland sea cumulative sea ice				-0,20		-0,04		-0,08

The general picture is one of a lack of significant correlation between FS ice export and Greenland winter sea ice maxima. It could be argued that there is a slight association of high FS winter ice export years with low values of Greenland winter maxima (Hilmer´s value is significant at the 5% value, while the remaining are close to the 10% significance value). This would agree with Schuchman et al (1998)´s findings that anomalously strong northerly winds over the Odden area are responsible for Odden decay, and it is such a climatology that would produce an enhanced FS ice export. Now, as mentioned above, the winter Greenland sea ice extent is primarily driven thermodynamically by the amount of sea ice that is produced locally in the Odden, and thus one may be led to think that it is not influenced by the amount of sea ice exported through the Fram Strait and subsequently advected along the EGC. However, as Comiso et al (2001) point out, the presence of a shallow cold layer of fresh water on the surface provides the conditioning that facilitates the formation of sea ice in the area, and go on to say that ´if the average fluxes of only August and September are used to correlate with average Odden area during the following months, the relationship is positive, and the correlation coefficient is about 0.31. The correlation is not high but is significant´. The correlations computed above for FS in August and September and the following winter Greenland sea ice extent are not significant. Furthermore, Comiso et al had

a dataset of 20 years (1979-1998), which would thus require a correlation value of 0.37 to be significant at the 5% level. It is also noted that Comiso et al do not specify what months for Odden area they used. However, considering the Odden does not generally form till late November / early December (see Toudal 1999), I computed the correlation values for a cumulative sea ice area in the Greenland sea from early December to late February (see table 19 above). No significant correlations were found.

Geographical forcing of sea ice variability in the North Atlantic region.

The North Atlantic is well known for having some of the highest sea ice yearly variability regions in the Arctic/subarctic. This is not only confined to sea ice but other climatological parameters. This is a result of the several ways in which the geography makes the Atlantic ocean liable to greater changes of poleward transport of heat, and therefore of climate, than the other oceans (Lamb, 1979): firstly, the roughly north-south arrangement of the limits of the Atlantic ocean guides the currents into directions which have prominent northward and southward components; secondly, there are wide open connections with both the Arctic and Antarctic oceans. The inflow and outflow of water exchanged between the Arctic and Atlantic oceans are approximately ten times greater than the flow through the Bering Strait between the Arctic and Pacific. Among the changes of prevailing temperature in the course of the last century, some of the greatest have been over the northernmost Atlantic and those parts of the Arctic reached at times by North Atlantic drift water and the winds that have blown over it. Both in the warming and cooling periods around 1920 and 1960 respectively, the changes were particularly great along an axis through the Norwegian Sea and Barents Sea, increasing to a maximum over the farthest limits reached by the warm saline Atlantic water at the surface in the eastern Barents Sea. The highly variable climate of the North Atlantic has an imprint on sea ice variability, which is greater in the Atlantic sector than in the Pacific, while the region of maximum sea ice variability in the Northern Hemisphere is the Odden (Deser et al, 2000).

Atmospheric conditions for high and low sea ice episodes.

Mean winter (December through to February) SLP fields are computed for winters with sea ice cover greater than plus one standard deviation and less than minus one standard deviation, together with the difference between the two composites. The results are shown in Figure 27. Sea ice maxima (minima) in the Barents and Greenland seas are associated with a weaker (stronger) than normal Icelandic low pressure and its associated Norwegian sea trough. Sea ice conditions in the Labrador Sea (both north and south) and the south east Greenland sea show an opposite association with mean SLP to the Barents and Greenland. From the SLP difference maps, it immediately becomes apparent that the Barents and Greenland seas are negatively correlated with the NAO, while the opposite holds true for the Labrador and S. E. Greenland seas.

i) ii) iii)

Figure 27.a Barents i)max, ii)min, iii)diff, and below, 27.b Greenland i)max, ii)min, iii) dif

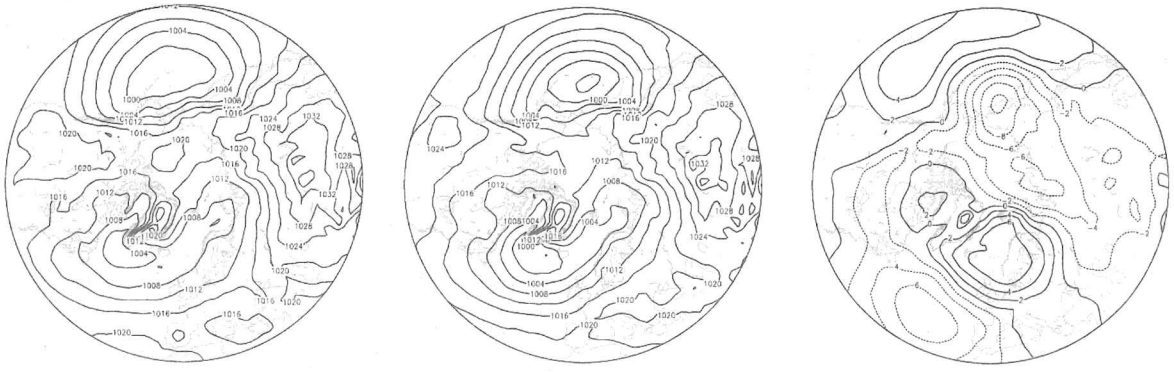

i) ii) iii)

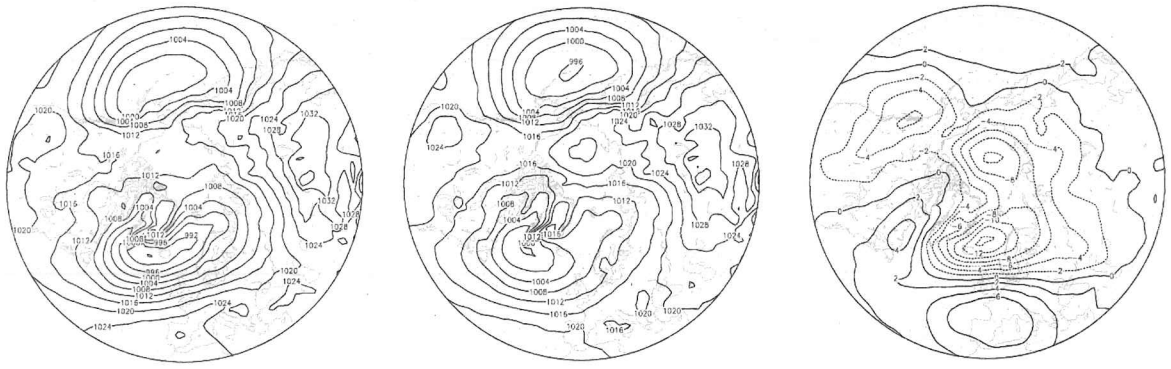

i) ii) iii)

27.c. Southeast Greenland, i)max, ii)min, iii) diff

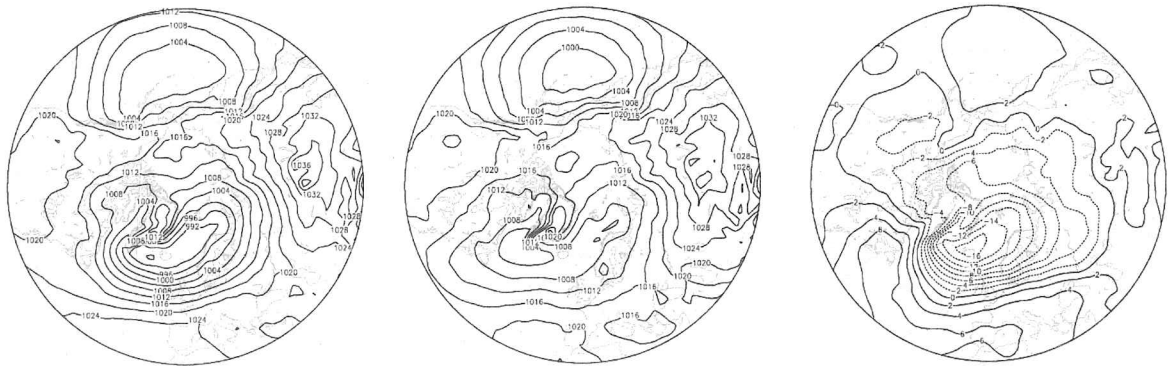

i) ii) iii)

27.d. Labrador North, i)max, ii)min, iii)diff

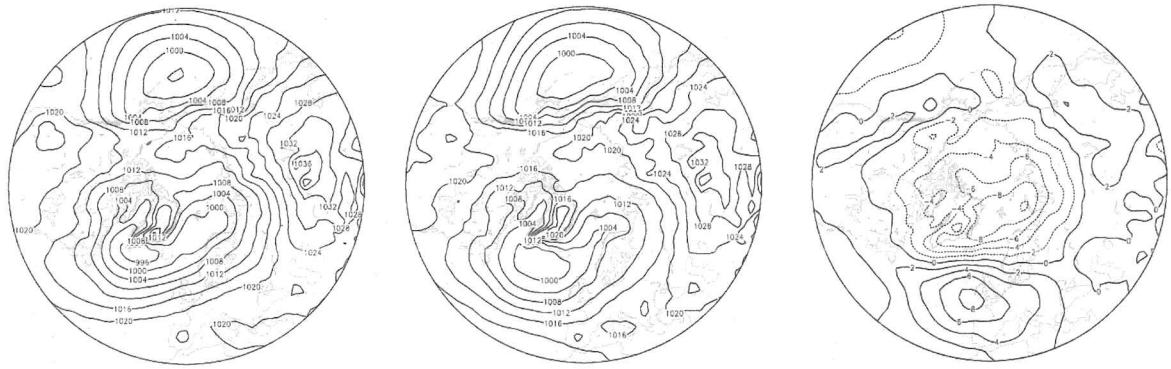

i) ii) iii)

27.e Labrador South, i)max, ii)min, iii)diff

Table 20 shows the correlation coefficients for the NAO index with winter sea ice maxima and integrated winter sea ice area. Several winter monthly combinations of NAO were used for the computations, only the ones that yielded the highest correlation are shown.

Table 20

Correlation coefficients for winter NAO index and sea ice extent. One asterisk indicates statistical significance at the 5% level, two indicate significance at the 1% level

Winter sea ice maxima					
NAO index	Barents	Greenland	Lab. N.	Lab. S.	S. E. Green
DJFM	-0,47**	-0,54**	0,45*	0,21	0,53**
Optimal for each area	-0,47** (DJFM)	-0,65** (NDJF)	0,49** (NDJFMA)	0,34* (JFM)	0,64** (JFM)
Winter integrated area, December to April					
NAO index	Barents	Greenland	Lab. N.	Lab. S.	S. E. Green
DJFM	-0,34*	-0,40*	0,42*	0,31	0,51**
Optimal for each area	-0,34* (DJFM)	-0,58** (NDJF)	0,51** (NDJF)	0,44*	0,56 ** (DJF)

Taking into consideration that temperature fluctuations over the Labrador region and the adjacent North American landmass are primarily driven by the NAO, the general lack of significant correlation between the Labrador south sea ice cover and the NAO index agrees with the above analysis that sea ice fluctuations in this area are primarily driven by the variations in the previous winter in the Labrador north sea ice extent, rather than atmospheric forcing. This agrees with Deser et al (2002) results; this work also showed that sea ice anomalies in the northern Labrador sea are a combination of atmospheric forcing and previous spring-summer salinity anomalies in the West Greenland current, with low (high) salinity anomalies leading positive (negative) sea ice anomalies by about 8 months. The significant correlation found between Southeast Greenland sea ice extent and the following year's northern Labrador sea ice is thus most likely a result of salinity modulation through the input of fresh water as the sea ice melts in the West Greenland current. The inverse relationship between the Barents sea ice cover and NAO index also agrees with previous work (e.g. Deser et al, 2000). To the author´s knowledge, the sea ice in the southern third of the EGC (what is labelled here as south east Greenland sea) has not been previously

researched *per se*, and has usually been included in the Greenland area if at all. Given that sea ice extent in the Greenland sea is almost an order of magnitude larger than that in Southeastern Greenland, coupled with the low variability of south Greenland sea ice, it is thus advisable to study the SE Greenland on its own. The shift in the sea ice –NAO relationship between the SEG and Greenland has not been previously reported. The south east Greenland-NAO relationship agrees with Hurrell and van Loon (1997)´s results using surface temperatures and SSTs, that high (low) index NAO winters are associated with cooler (warmer) than normal winters in south east Greenland. Unfortunately, they report insufficient data coverage for analysis in the Greenland sea region proper. Considering the above results, an intriguing question arises. If the Greenland sea and the SEG show opposite relationships with the NAO, why is that the sea ice extents in both areas are not significantly negatively correlated (see table x above)? One of the explanations may be that the NAO, while being significantly correlated with sea ice area in both regions, still only accounts for around 40-45 % of the variance at best, so there is a large amount of variability that is driven by other factors (e.g. oceanic variations, or other atmospheric teleconnection patterns). Another possibility is born out of the fact that the NAO does show a tendency to remain in one phase or another for a number of years, e.g. positive phase from 1989 to 1995, low phase from 1985 to 1988, or the negative phase years during the 1960s. The 1-year autolag correlation for the period 1979-2001 is found to be r=0,27, which if 1996 is ignored rises to r=0,45 (1995 to 1996 saw the biggest recorded shift in winter NAO index). Given this behaviour of the NAO, an arbitrary year X with a positive NAO will statistically lead to negative anomalies in sea ice extent in the East Greenland sea, and positive anomalies in the SEG. The following year, it will be more likely that the NAO index is in a positive phase, and thus although the atmospherically forced anomalies in the SEG will be positive, considering that the travel time along the EGC of sea ice from the East Greenland sea to the SEG is about 1 year, an oceanic negative forcing anomaly will result from the low sea ice concentration the previous year in the East Greenland sea.

The one area where the above reported correlations come into conflict with previous results is the Greenland sea, although it has been previously researched in the context of Odden variability rather than Greenland sea *per se*. To address this difference the Odden sea ice extent was computed. This has previously been done in two different ways. Schuchman et al (1998) substract the pre-Odden ice covered area in the Greenland Sea from the ice concentration maps. This is done for every year and is determined by averaging all of the total ice concentration estimates for the month of October. This month is chosen for calculating the initial winter ice edge because this is approximately the time of minimum ice extent, and the Odden does not begin to form until November or later. Later work has focused on defining an Odden 'boxed area' that remains constant throughout the years. Although different workers have used slightly different areas (e.g. Comiso et al, 2001; Toudal, 1999) these differences have not resulted in any conflicting results in terms of Odden area and variability. The Odden 'boxed area' used in this work is shown in Figure 28.

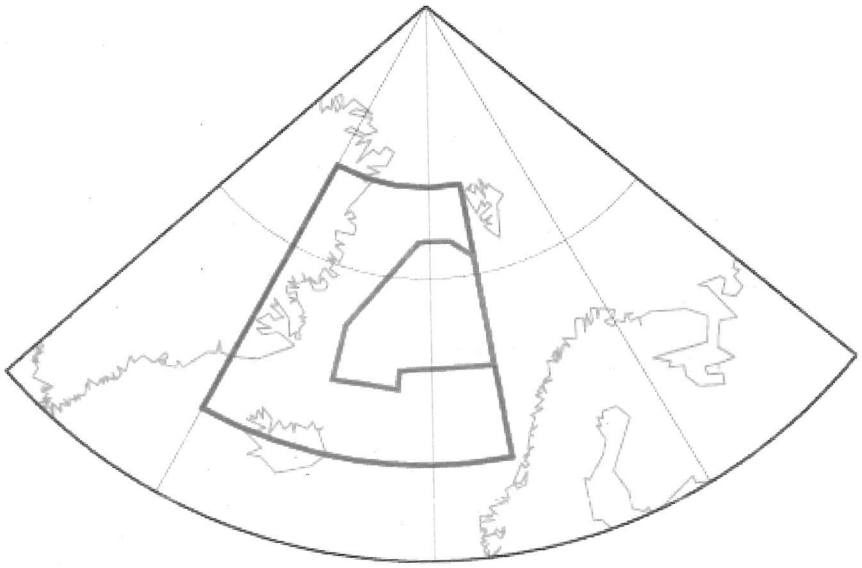

Figure 28. Odden boxed area (red) and Greenland Sea boxed area (blue, 2 in Fig 23)

Schuchman et al (1998) report that 'the correlation between the NAO index and the annual maximum area covered by Odden ice was r= 0.42, not statistically significant at the 0.95 level' .Comiso et al (2001) report a correlation coefficient of 0.4 of NAO index and Odden extent, although they do not specify the time resolution of either variable. Chasmer (2001)

found a varying correlation of -0.08 (1978 to 1983), 0.25 (1984 to 1989), 0.67 (1989 to 1993) and -0.46 (1994 to 1996) between the NAO index and a wavelet transform set of sea ice concentrations, and concluded that 'when the NAO is in positive mode, sea ice concentrations increase'.

Table 21 shows the correlation found by this author between winter NAO index and Odden sea ice extent.

Table 21

Corrrelation coefficients for winter NAO index and Odden sea ice extent.

NAO Index	Maximum extent	Dec-Apr	Oct-May	Dec-Feb
DJF	-0,69	-0,61	-0,61	-0,47
Optimal for each area	-0,69 (DJF)	-0,62 (NDJF)	-0,65 (NDJF)	-0,50 (NDJF)

As expected from the results yielded for the Greenland sea, the Odden is negatively correlated with the NAO winter index, and the coefficients are in fact greater than those for the Greenland sea. All values are significant to the 1% level.

Figure 29 Winter (DJF) NAO index and Odden maximum sea ice extent in hundreds of thousands of km^2.

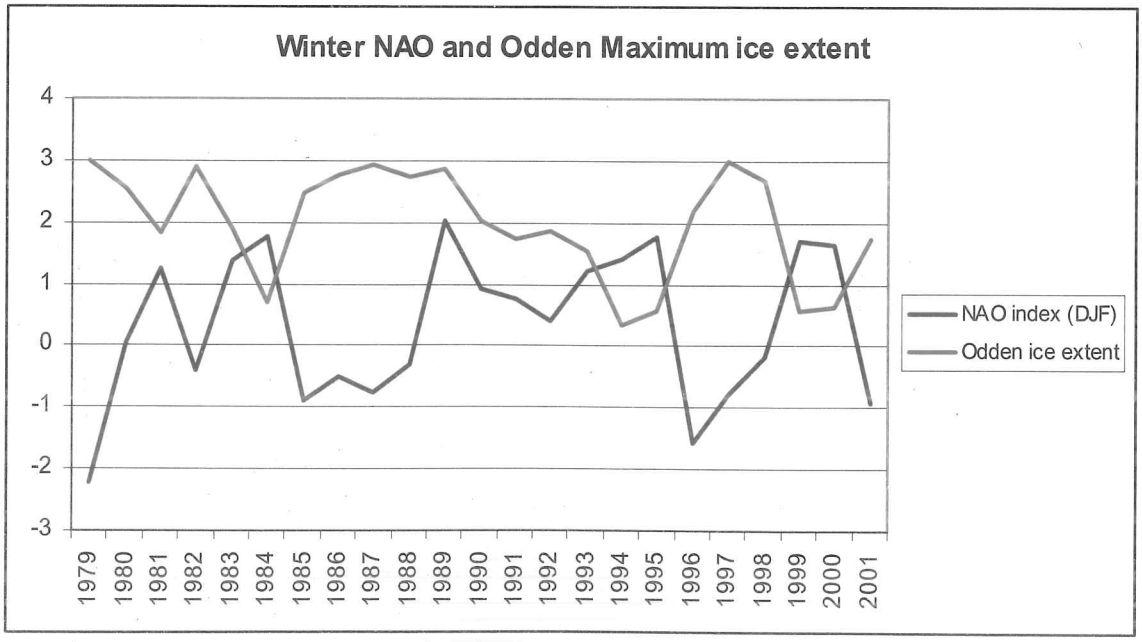

It is clear that the negative correlation between both variables is continuous throughout the whole period. The one major exception is 1989, where a large positive NAO index and a large Odden sea ice extent occur (see figure 30 below).

Figure 30. Scatter plot of winter NAO index and Odden yearly maximum

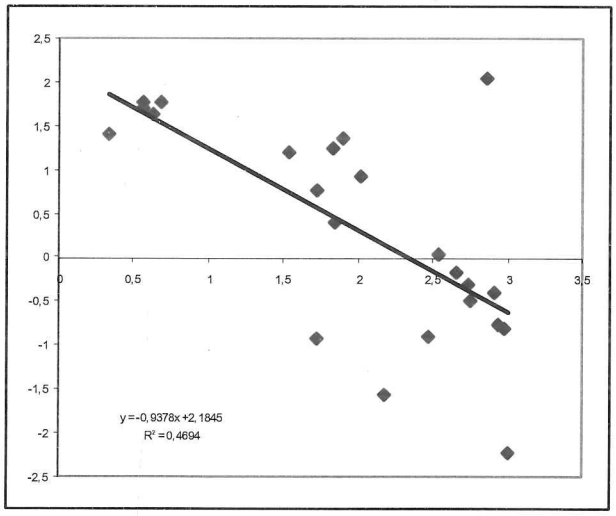

Excluding 1989 from the NAO – Odden correlation analysis above, the correlation coefficient becomes r=-0,81 for sea ice extent maxima, r=-0,78 for December to April integrated sea ice extent and r=-0,79 for October to May integrated sea ice extent. Given these very large correlation figures, it is puzzling that previous authors have found opposite results. I do not believe that it is a combination of shorter records and the exceptional year of 1989 as the correlation for 1979-1995 (the dataset Schuchman et al had access to) for DJF NAO and Odden yearly maximum extent is r=-0.69.

I will now show that there is ample evidence that agrees with a true negative relationship between the NAO index and the Odden.

Firstly, Schuchman et al (1998) performed an analysis using interpolated in situ buoy meteorological data to determine the atmospheric conditions which are associated with Odden formation, decay, stagnation or absence. The data available, from the International Arctic Buoy Program, were surface air temperature, surface air pressure and geostrophic wind speed and direction. It was found that temperature and wind are both related to Odden ice formation while atmospheric pressure *per se* was not. They found that Odden formation

occurs when winds are moderate and out of the west, bringing very cold air from the Greenland ice sheet. At the other end of the spectrum, Odden decay is associated with very high winds from the north / northeast. It is theorized that decay occurs through the combination of increased melting and mechanical destruction at the ice edge. The northerly and northeasterly winds transport both ice and water to the southwest; however, because the ice is rougher, it moves faster than the underlying water. At the southern edge of the Odden the ice moves out into the relatively warm open Greenland sea and rapidly melts. The mean SLP fields during high and low NAO phases (see above) show that during low NAO winters, the mean geostrophic flow over the Odden region is northwesterly, while during high NAO winters, it becomes of northerly direction, with a pressure gradient that is about twice that for the low NAO winters, leading to higher wind velocities. Thus a low (high) NAO phase SLP approximates the Odden growth (decay) regime of Schuchman et al (1998). The SLP difference composite map (Figure 4.iii) show that during the negative NAO phase winters, the anomalous wind set up with respect to positive phase NAO winters is westerly and vice versa, implying greater number of outbreaks of cold air from Greenland over the Odden region during negative NAO winters. Moreover, this study found that storms passing overhead the Odden region were responsible for large decays in Odden area over a period of just a few days. Considering the storm track over the North Atlantic during positive and negative phase NAO winters, the frequency of storms over the Odden region will be greater during positive NAO winters (Rogers, 1997).

Secondly, a particularly significant positive sea ice anomaly took place in the Greenland sea during 1963-1972, reaching a climax in 1968 (Mysak and Manak, 1989). Sea ice reached the East Iceland current and the east coast of Iceland for the first time since 1919 (Lamb, 1979), while the Odden reached then what is considered to be its greatest 20th century extent (Vinje, 2001). These years coincide with the greatest recorded negative departure of the NAO index. Other years in which sea ice extent in the Greenland sea (and by default the Odden) has been

reported to be anomalously large are 1918 and 1919, and 1888 (Lamb, 1979). In all these years the NAO is markedly negative (see Figure 5 above)

Thirdly, Shuchman et al. (1998), show that there is a significant negative correlation between winter temperatures in Jan Mayen and Odden extent. Jan Mayen is a small volcanic island located in the Greenland sea at 71N and 10W. The temperature record there extends to 1921. The correlation between December to March temperature and NAO index is r=0.34. Running means of 15 year and 30 year correlations show that the correlation has been significantly positive throughout the record, especially so during the early and late 20th century.

Finally, taking full advantage of the weekly resolution of sea ice data, periods of rapid Odden growth and decay are identified and the mean SLP during those time periods is computed. The periods of rapid growth and decay are calculated sequentially throughout the whole data set for 4 week periods, as this is the closest time period to a month (see Table A in the appendix).

Considering that the average size of the Odden remains almost constant from early January to early April (Toudal, 1999), and that the late winter season decay periods in April and May are probably forced by the seasonal increase in solar radiation rather than atmospheric circulation variability, the major periods of decay prior to mid April are also computed and assumed to be caused primarily by atmospheric variability. The mean SLP fields during growth periods over 1 standard deviation (s.d.) of the annual maximum growth period average and during decay periods greater than 1 s.d., of the annual maximum decay period average are calculated. These are the growth periods for the winters of 1982, 1986, 1989, 1990 and 1997; and the decay periods for the winters of 1988, 1990 and 1998.

Fig 31. Mean SLP fields for Odden i) growth, ii) decay events, and iii) difference between the composites

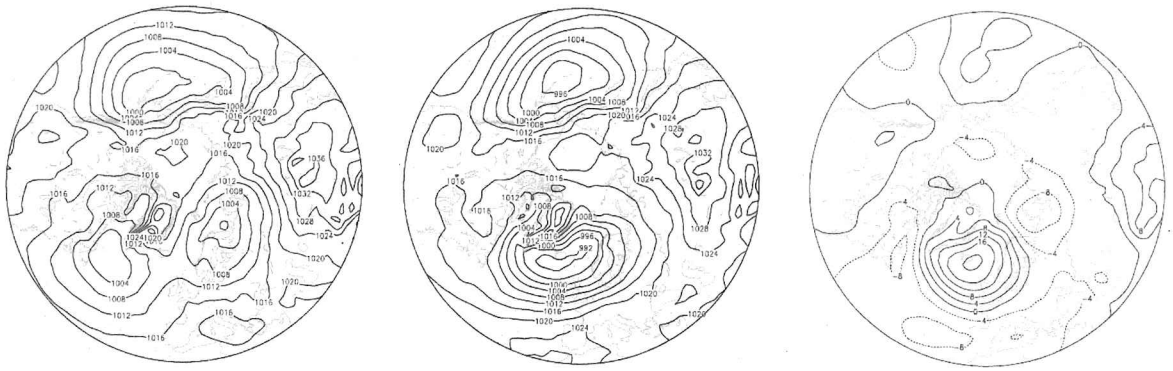

i) ii) iii)

The mean SLP field for growth events show remnants of a negative NAO like configuration, with a well developed Barents Low. The Norwegian Sea trough is absent and there is little connectivity with a weakened, southwesterly displaced Icelandic Low. During Odden decay events, the mean SLP field shows a positive NAO like configuration, with a unique, deep centre of low pressure in the North Atlantic and a well developed Norway Sea trough. The SLP difference map shows a close resemblance with the difference map for the Greenland sea difference SLP above in figure 27.b. An interesting feature of the pressure distribution in Figure 31.iii., is that rather than a dipole-like structure it shows mainly a mono-pole configuration, with a centre of action over Iceland.

Polar vortex derived index and sea ice fluctuations

The tropospheric teleconnection patterns that arise during strong polar vortex episodes (see above) and their associated 850 hPa wind anomalies are expected to show a link with Odden extent fluctuations. From inspection of figure 21, a positive phase NA-SVR resembles the Odden decay SLP above, with a strong southerly advection of mild, Atlantic type air masses onto the Odden region. During the negative phase NA-SVR, a moderate northwesterly advection of cold Polar type air masses should be inductive to Odden growth. Although in neither case the anomalous 850 hPa wind field is significant to the 95% significance level

over the Odden region, there are large areas of significant anomalous wind immediately to the south in the positive phase and both to the south and north in the negative phase, and so some degree of correlation is expected. Thus, for all winter months with a strong polar vortex, the correlation between the 300hPa NA-SVR index and the change in Odden extent anomaly for that particular month are computed and results in r = -0.28 (significant to the 0.95 level). The correlation between the NAO index and Odden extent change is also computed, to address whether the polar vortex derived teleconnection index has a higher capacity to reflect Odden extent changes than the NAO index. The resulting correlation is r = -0.37 (significant to the 0.99 level). One shortcoming of this analysis is that to some degree the monthly changes in Odden extent are dependant on the initial condition of the Odden. Given the quasi constant average Odden extent from early January till early April, an Odden extent close to zero at the beginning of the month (and thus anomalously negative) will be likely to remain close to zero at the end of the month and show a similar negative anomaly during a positive NAO month / positive phase of the NA-SVR, yielding no significant change in Odden extent anomaly. The same ´no change in Odden anomaly´ scenario would occur as a result of an upper limit in the extent of the Odden (of around 300,000 km2, Schuchman et al 1998; 250,000km2, Toudal 1999- dependant on Odden 'boxed area'). Thus an initial large Odden extent (and thus anomalously positive) followed by a negative NAO / negative phase of the NA-SVR would lead to an equally large Odden extent anomaly. During the weak polar vortex regime, the lack of significant change in 850 hPa winds between polarities of the teleconnection patterns over the Odden and adjacent areas may lead one to think that no correlation may be found between these indexes and Odden extent. However, the strong correlation of the eastern NA-WVR index with the classical NAO index (r=0.91, Graf and Walter, 2005), and the proximity of the northern centre of action to the Odden region, means that a significant negative correlation may be expected. The correlation between NAO, eastern NA-WVR and western NA-WVR with Odden extent are computed during all weak polar vortex months in the same manner as for strong vortex

regime described above. The resulting correlations are r = -0.58 for eastern NA-WVR, r = -0.52 for NAO and r = 0.14 for western NA-WVR. Only the first correlation is significant to the 95 % level, although given the low sample number (there are just 19 months of weak polar vortex from 1978 to 2001) these results have to be taken cautiously. Nevertheless, this raises the issue whether the eastern NA-WVR index may have more explanatory power over the Odden extent than a classical NAO index. The correlation between eastern NA-WVR index for December to February and Odden winter maximum extent is r=-0.59, while it is r=-0.69 for DJF NAO (see table x above), as one would expect, since the teleconnection pattern only appears for weak polar vortex regimes rather than at all times.

Given the possibility that a vortex strength derived teleconnection pattern may be more appropriate for use than the classical NAO index for the appropriate months, the above analysis is carried out for all areas.

Table 22

Correlation coefficients for changes in extent anomaly during months of strong polar vortex with the classical NAO index and the NA-SVR upper troposphere index. One asterisk indicates statistical significance at the 5% level, two indicate significance at the 1% level

	Odden	Barents	Greenland Sea	Labrador North	Labrador South	SoutheastGreenland
NAO	-0,37**	-0,38**	-0,58**	0,35**	0,50**	-0,09
NA-SVR	-0,28*	-0,23	-0,57**	0,44**	0,54**	-0,10

There is a pattern for higher NAO correlation in the eastern regions (Barents, Greenland Sea and Odden), and higher NA-SVR correlations in the Labrador seas. The ice extent in southeast Greenland shows no significant correlation with either index. These results agree with the patterns of anomalous 850 hPa field in Figure 21. The only area considered in this study for which the wind anomalies exceed the 99 significance level is the Labrador sea (both north and south) and the directions are such that in the positive phase of the NA-SVR,

cold airmasses from the Canadian Arctic advect onto the Labrador sea, while during the negative phase mild Atlantic airmasses are advected.

Table 23

Correlation coefficients for changes in extent anomaly during months of weak polar vortex with the classical NAO index and the NA-SVR upper troposphere index. One asterisk indicates statistical significance at the 5% level, two indicate significance at the 1% level

	Odden	Barents	Green.	LabN	LabS	SG
NAO	-0,52*	-0,51*	-0,61**	0,63**	0,06	0,10
East NA-WVR	-0,58**	-0,46*	-0,68**	0,54*	0,10	-0,04
West NA-WVR	-0,14	-0,49*	-0,19	0,65**	0,15	0,44*

During the weak vortex regime, the eastern NA-WVR shows similar values to the classical NAO, while the western NA-WVR shows strong influence in the northern Labrador sea, southeast Greenland and the Barents sea. It is rather remarkable that the Barents sea should show such response with the western teleconnection patterns considering the distance to the centres of action and the fact that closer regions (e.g. the Greenland sea) show no such response. The results nevertheless agree with the anomalous wind fields in 21, with anomalous northeasterly (southwesterly) wind vectors (?) during the negative (positive) phase inducing sea ice growth (decay), thus resulting in a negative correlation. The lack of correlation with the southern Labrador reflects the above mentioned strong oceanic forcing of sea ice variability in the region.

Conclusion

This work shows the link between Fram Strait ice export and planetary wave 1 phase to be significant for all months of the year for modelled FS ice export data, while the winter relationship between w1 phase and export remains quasi stationary. Observational data does

not show as significant a link with the w1 phase but shows similarities with the modelled data in the monthly variation of such link (namely maximum values in January and August). The link of Fram Strait export with the phase of the NAO is shown to have become significant only since the late 1970s, in accordance with previous results. Observational data thus shows smaller coupling to atmospheric variability than modelled data, which is to be expected due to the nature of the models.

This work also shows Fram Strait ice flux to be coupled with other environmental variables, such as Svalbard glacier mass balance and Greenland sea summer ice extent, due to direct factors (such as winter ice flowing through the Fram Strait susbsequently becoming summer sea ice in the Greenland sea) or indirect factors (such as an atmospheric pattern that is conducive both to enhanced summer Fram Strait flux and low summer ablation in Svalbard). This opens up the possibility of proxy measurements.

Sea ice fluctuations in the North Atlantic / Arctic are modulated to a large extent by the NAO. A distinction can be made however between regions depending on whether atmospheric or oceanic forcing is the main agent of variability. The Odden, region of largest sea ice interannual variability in the Northern Hemisphere, is shown to be strongly influenced by the NAO, and to be *negatively* correlated to the index rather than positively as previous studies had proposed.

The state of the stratospheric polar vortex is shown to bear some influence on sea ice conditions, both in terms of the *de facto* polar vortex strength and the upper troposphere teleconnection patterns that arise depending on the state of the vortex. This influence ranges from the barely discernible (e.g. vortex strength and FS ice export) to relationships that show a higher degree of correlation than a classical NAO index. However, given that the stratosphere is only in a weak or strong vortex for discrete amount of times, a NAO index may be more suitable for continuous analysis of sea ice fluctuations, whereas polar vortex derived indices may be used for discrete time case studies.

Bibliography

Ambaum, M.H.P., B.J. Hoskins, and D. B. Stephenson, 2001: Arctic Oscillation or North Atlantic Oscillation?, *Journal of Climate*, **14**, 3495-3507.

Armstrong, R.L. and M.J. Brodzik. 2002: Northern Hemisphere EASE-Grid weekly snow cover and sea ice extent version 2. Boulder, CO, USA: National Snow and Ice Data Center. CD-ROM.

Baldwin, M. P., X. Cheng and T. J. Dunkerton, 1994: Observed correlations between winter-mean tropospheric and stratospheric anomalies, *Geophysical Research Letters*, **21**, p1141-1144.

Baldwin, M. P., and T. J. Dunkerton, 1999: Propagation of the Arctic Oscillation from the stratosphere to the troposphere, *Journal of Geophysical Research*, **104**, 30,937-30,946.

Baldwin, M. P., and T. J. Dunkerton, 2001: Stratospheric harbingers of anomalous weather regimes, *Science*, **294**, p581-584.

Baldwin M.P., D. W. Thompson, E. F. Shuckburgh, W. A. Norton, N. P. Gillett, 2003: Weather from the stratosphere?, *Science*, **301**, 317-319.

Blanchard, E., 2003: On the relationships between glacier mass balance and climate in the eastern North Atlantic and teleconnections with the North Pacific, unpublished BA thesis, University of Cambridge, UK.

Castanheira, J.M. and H.-F. Graf, 2003: North Pacific - North Atlantic relationships under stratospheric control?, *Journal of Geophysical Research*, **108**, D1, 4036, doi :10.1029/2002JD002754, 2003

Cavalieri, D. J., 2002: A link between Fram Strait sea ice export and atmospheric planetary wave phase, *Geophysical Research Letters*, **29** (12), 2002.

Cavalieri, D. J., J. P. Crawford, M. R. Drinkwater, D. T. Eppler, L. D. Farmer, R. R. Jentz, and C. C. Wackerman, 1991: Aircraft active and passive microwave validation of sea ice concentration from the DMSP SSMI, *Journal of Geophysical Research*, **96**, c12, p21,989-22,008.

Cavalieri, D. J., and S. Häkkinen, 2001: Arctic climate and atmospheric planetary waves, *Geophysical Research Letters*, **28**, 791-794.

Chasmer, L., 2001: Interactions between the North Atlantic Oscillation and the Odden sea ice peninsula: Greenland sea, Masters Research, University of Waterloo, Canada.

Chapman, W. L. and J. E. Walsh, 1993: Recent variations of sea ice and air temperatures in high latitudes, *Bulletin of the American Meteorological Society*, **74**, no. 1.

Christiansen, B., 2003: Evidence for nonlinear climate change: Two stratospheric regimes and a regime shift, *Journal of Climate*, **16**, 3681-3689.

Comiso, J. C., P. Wadhams, L. T. Pedersen and R. A. Gersten, 2001: Seasonal and interannual variability of the Odden ice tongue and a study of environmental effects, *Journal of Geophysical Research*, **106** (C5), p9093-9116.

Deser, C., 2000: On the teleconnectivity of the Arctic Oscillation, *Geophysical Research Letters*, **27**, 6, 779-782.

Deser, C., J. E. Walsh and M. S. Timlin, 2000: Arctic sea ice variability in the context of recent atmospheric circulation trends, *Journal of Climate*, **13**, 617-633.

Deser, C., M. Holland, G. Reverdin and M. S. Timlin, 2002: Decadal variations in Labrador sea ice cover and North Atlantic sea ice temperatures, *Journal of Geophysical Research*, **107**, 10.1029/2000JC000683.

Dickson, R. R., T. J. Osborn, J. W. Hurrell, J. Meincke, J. Blindheim, B. Adlandsvik, T. Vinje, G. Alekseev, and W. Maslowski, 2000: The Arctic Ocean response to the North Atlantic Oscillation, *Journal of Climate*, **13**, 2671- 2696.

Gloersen, P., and W. J. Campbell, 1991: Recent variations in Arctic and Antarctic sea ice covers, *Nature*, **352**, p33-36.

Graf, H-F., and K. Walter, 2005: Polar vortex controls coupling of North Atlantic ocean and atmosphere, *Geophysical Research Letters*, **32**, L01704.

Häkkinen, S., and C. A. Geiger, 2000: Simulated low frequency modes of circulation in the Arctic Ocean, *Journal of Geophysical Research*, **105**, 6549-6564.

Hartley, D.E., J. Villarin, R.X. Black, and C.A. Davis, 1998: A new perspective on the dynamical link between the stratosphere and troposphere, *Nature*, **391**, 471-474.

Hilmer, M., 2001: A model study of Arctic sea ice variability, Thesis, Institüt fur Meereskunde of the Christian-Albrechts-Universität Kiel, Germany.

Hilmer, M., and T. Jung, 2000: Evidence for a recent change in the link between the North Atlantic Oscillation and Arctic sea ice export, *Geophysical Research Letters*, **27**, 989-992.

Hurrell, J.W., 1995: Decadal trends in the North Oscillation: regional temperatures and precipitation, *Science*, **269**, 676-679.

Hurrell, J. W., and H. van Loon, 1997: Decadal variations in climate associated with the North Atlantic Oscillation, *Climatic Change*, **36**, 301-326.

Kwok, R., and D. A. Rothrock, 1999: Variability of Fram Strait ice flux and North Atlantic Oscillation, *Journal of Geophysical Research*, **104**, 5177-5189.

Labitzke, K., 1987: Sunspots, the QBO, and the stratospheric temperature in the North Polar-region, *Geophysical Research Letters*, **14**, 535-537.

Labitzke, K., and H. van Loon, 1988: Associations between the 11-year solar cycle, the QBO, and the atmosphere. Part I: the troposphere and stratosphere in the Northern Hemisphere winter. J. Atmos. Terr. Phys., **50**, 197-206.

Lamb, H. H., 1979: Climatic variation and changes in the wind and ocean circulation: the Little Ice age in the Northeast Atlantic, *Quaternary Research*, **11**, 1-20.

Matsuno, T., 1970: Vertical propagation of stationary planetary waves in the winter Northern Hemisphere. *Journal of Atmospheric Science*, **27**, 871-883.

Mysak, L., and D. K. Manak, 1989: Arctic sea ice extent and anomalies, 1953-1984, *Atmosphere-Ocean*, **27**, 376-405.

Mysak, L., and S. A. Venegas, 1998: Decadal climate oscillations in the Arctic: a new feedback loop for atmosphere-ice-ocean interactions, *Geophysical Research Letters*, **25**, 3607-3610.

Parkinson, C. L., D. J. Cavalieri, P. Glorsen, H. J. Zwally and J. C. Comiso, 1999: Arctic sea ice extents, areas, and trends 1978-1996, *Journal of Geophysical Research*, **104**, C9, p20,837-20,856.

Perlwitz, J., and H-F. Graf, 1995: The statistical connection between tropospheric and stratospheric circulation of the Northern Hemisphere in winter, *Journal of Climate*, **8**, 2281-2295.

Perlwitz, J., and H-F. Graf, 2001: Troposphere-stratosphere dynamic coupling under strong and weak polar vortex conditions, *Geophysical Research Letters*, **28**, 271-274.

Rogers, J. C., 1997: North Atlantic storm track variability and the North Atlantic Oscillation and climate variability of northwest Europe, *Journal of Climate*, **10**, 1635-1647.

Rogers, J.C., and M. J. McHugh, 2002: On the separability of the North Atlantic oscillation and Arctic oscillation, *Climate Dynamics*, **19**, 599-608.

Schuchman, R. A, E. G. Josberger, C. A. Russel, K. W. Fischer, O. M. Johannessen, J. Johannessen and P. Glorsen, 1998: Greenland Sea Odden sea ice feature: Intra-annual and interannual variability, *Journal of Geophysical Research*, **103** (C6), p12,709-12,724.

Schmith, T., and C. Hansen, 2003: Fram Strait ice export during the nineteenth and twentieth centuries reconstructed from a multiyear sea ice index from Southwestern Greenland. *Journal of Climate*, **16**, No. 16, pp. 2782-2792.

Thompson, D. W. J, and J. M. Wallace, 1998: The Arctic Oscillation signature in the wintertime geopotential height and temperature fields. *Geophysical Research Letters*, **25**, 1297-1300.

Toudal, L., 1999: Ice extent in the Greenland sea 1978-1995, *Deep Sea Research II*, **46**, 1237-1254.

van Loon, H., and Rogers, J. F., 1978. The seesaw in temperatures between Greenland and Northern Europe. Part I: general description. *Monthly Weather Review*, **106**: 296-310.

Venegas, S. A., and L. A. Mysak, 2000: Is there a dominant timescale of natural climate variability in the Arctic?, *Journal of Climate*, **13**, 3412-3434.

Vinje, T., N. Nordlund and A. Kvambekk, Monitoring ice thickness in Fram Strait, *Journal of Geophysical Research*, **103**, C5, 1998.

Vinje, T., 2001: Anomalies and trend of sea-ice extent and atmospheric circulation in the Nordic seas during the period 1864-1998, *Journal of Climate*, **14**, 255-267.

Vinje, T., 2001: Fram Strait ice fluxes and atmospheric circulation 1951-2000, *Journal of Climate*, **14**, 3508-3517.

Wadhams, P., 1990: Evidence for thinning of the Arctic ice cover north of Greenland, *Nature,* **345**, 795-797.

Wadhams, P., 1999: The Odden ice tongue and Greenland sea convection, *Weather*, **54**, p91-98.

Wadhams, P., and J. C. Comiso, 1999: Two modes of appearance of the Odden ice tongue in the Greenland sea, *Geophysical Research Letters*, **26**, 2497-2500.

Walker, G. T.,1923: Correlations in seasonal variations of weather, VIII: a preliminary study of world weather. Mem. Ind. Meteor. Dept. (Poona), **24**, 275-332.

Wallace, J. M. and Gutzler, D. S., 1981. Teleconnections in the Geopotential Height Field during the Northern Hemisphere Winter. *Monthly Weather Review*, **109**: 784-812.

Walter, K., and H-F. Graf, 2005: North Atlantic variability structure, storm tracks, and precipitation depending on the polar vortex strength, *Atmospheric Chemistry and Physics*, **5**, 239-248.

Walter, K., 2003: Changing patterns of tropospheric variability in the North Atlantic region, Thesis, Universität Hamburg, Germany.

Widell, K., S. Osterhus, and T. Gammelsrod, Sea ice velocity in the Fram Strait monitored by moored instruments, *Geophysical Research Letters*, **30**, 2003.

Appendix

Table A., Greatest four-week yearly periods of Odden growth and decay- (m/d) indicates month / day.

Increments						Decrements (complete winter)						Decrements (to 1st week of April)					
Winter	From (m/d)		To		Growth	Winter	From		To		Decay	Winter	From		To		Decay
1979	11	19	12	17	167,8	1979	4	15	5	13	-176,6	1979	3	4	4	1	-150,2
1980	1	20	2	17	140,1	1980	3	30	4	27	-124,4	1980	3	9	4	6	-101,2
1981	11	23	12	21	105,6	1981	2	1	3	1	-137,6	1981	2	1	3	1	-137,6
1982	11	22	12	20	228,7	1982	4	4	5	2	-181,6	1982	2	28	3	28	-134,5
1983	1	16	2	13	127,6	1983	3	20	4	17	-154,0	1983	2	6	3	6	-125,0
1984	11	13	12	11	56,6	1984	12	11	1	8	-65,4	1984	12	11	1	8	-65,4
1985	1	20	2	17	127,6	1985	4	21	5	19	-157,7	1985	11	25	12	23	-11,9
1986	11	24	12	22	179,1	1986	3	2	3	30	-100,5	1986	3	2	3	30	-100,5
1987	1	4	2	1	153,3	1987	3	29	4	26	-181,0	1987	3	8	4	5	-89,9
1988	2	14	3	13	140,8	1988	1	24	2	21	-186,0	1988	1	24	2	21	-186,0
1989	11	13	12	11	207,4	1989	3	19	4	16	-195,4	1989	1	29	2	26	-96,1
1990	11	19	12	17	173,4	1990	1	7	2	4	-159,0	1990	1	7	2	4	-159,0
1991	1	27	2	24	89,2	1991	4	7	5	5	-167,8	1991	12	23	1	20	-37,7
1992	12	15	1	12	101,2	1992	2	9	3	8	-120,6	1992	2	9	3	8	-120,6
1993	1	3	1	31	108,1	1993	2	21	3	21	-99,9	1993	2	21	3	21	-99,9
1994	2	6	3	6	33,9	1994	3	6	4	3	-33,3	1994	3	6	4	3	-33,3
1995	4	23	5	21	59,7	1995	11	13	12	11	-34,6	1995	11	13	12	11	-34,6
1996	3	17	4	14	77,3	1996	5	12	6	9	-73,5	1996	12	24	1	21	-20,1
1997	12	1	12	29	189,1	1997	3	23	4	20	-208,6	1997	1	26	2	23	-110,6
1998	1	4	2	1	94,9	1998	2	8	3	8	-203,0	1998	2	8	3	8	-203,0
1999	12	13	1	10	39,6	1999	1	10	2	7	-52,8	1999	1	10	2	7	-52,8
2000	4	2	4	30	40,8	2000	5	7	6	4	-61,6	2000	2	13	3	12	-25,1
2001	12	10	1	7	107,5	2001	3	4	4	1	-84,2	2001	3	4	4	1	-84,2